AD-A268 090

REPORT DOCUMENTATION PAGE

Form Approved
OMB No. 0704-0188

1. AGENCY USE ONLY (Leave blank)	2. REPORT DATE	3. REPORT TYPE AND DATES COVERED
	1993	THESIS/DISSERTATION

4. TITLE AND SUBTITLE
Mesoscale Precipitation Systems in Winter Storms

5. FUNDING NUMBERS

6. AUTHOR(S)
Mark A. Kaster

7. PERFORMING ORGANIZATION NAME(S) AND ADDRESS(ES)
AFIT Student Attending: St Louis University

8. PERFORMING ORGANIZATION REPORT NUMBER
AFIT/CI/CIA-93-023

9. SPONSORING / MONITORING AGENCY NAME(S) AND ADDRESS(ES)
DEPARTMENT OF THE AIR FORCE
AFIT/CI
2950 P STREET
WRIGHT-PATTERSON AFB OH 45433-7765

10. SPONSORING / MONITORING AGENCY REPORT NUMBER

11. SUPPLEMENTARY NOTES

12a. DISTRIBUTION / AVAILABILITY STATEMENT
Approved for Public Release IAW 190-1
Distribution Unlimited
MICHAEL M. BRICKER, SMSgt, USAF
Chief Administration

12b. DISTRIBUTION CODE

13. ABSTRACT (Maximum 200 words)

93-19321

14. SUBJECT TERMS	15. NUMBER OF PAGES 101
	16. PRICE CODE

17. SECURITY CLASSIFICATION OF REPORT	18. SECURITY CLASSIFICATION OF THIS PAGE	19. SECURITY CLASSIFICATION OF ABSTRACT	20. LIMITATION OF ABSTRACT

DISCLAIMER NOTICE

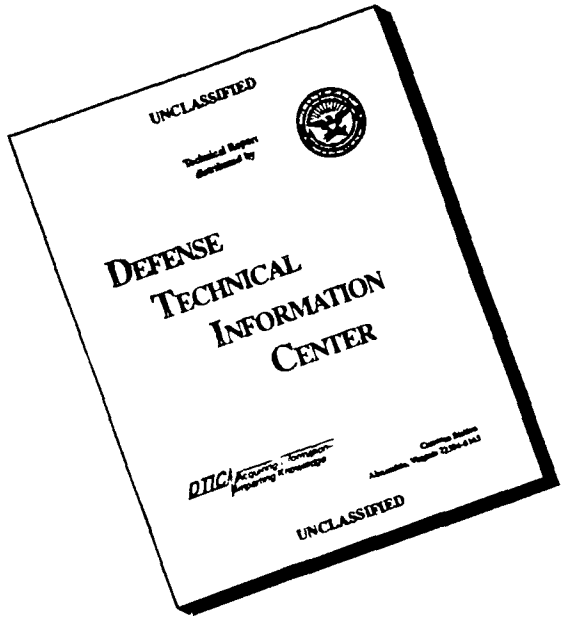

THIS DOCUMENT IS BEST QUALITY AVAILABLE. THE COPY FURNISHED TO DTIC CONTAINED A SIGNIFICANT NUMBER OF PAGES WHICH DO NOT REPRODUCE LEGIBLY.

MESOSCALE PRECIPITATION SYSTEMS IN WINTER STORMS

Mark Arthur Kaster, B.S.

A Digest Presented to the Faculty of the Graduate School of Saint Louis University in Partial Fulfillment of the Requirements for the Degree of Master of Science (Research)

1993

DIGEST

Heavy frozen precipitation produced by complex mesoscale patterns embedded within winter extratropical cyclones (ETCs) adversely affect many areas of the United States each year. The initiation, organization, and movement of these mesoscale precipitation systems (MPSs) within ETCs needs to be studied to more accurately predict these events. This study focuses on developing diagnostic techniques from synoptic scale datasets, which help to isolate those forcing mechanisms responsible for MPS events within larger scale precipitation regimes.

Constant pressure and isentropic datasets are used to explore the structure of numerous frozen precipitation events occurring during the 1987-1992 winter seasons. Specifically, selected case studies from this time period are used to illustrate how conditional symmetric instability (CSI), elevated convection, frontogenetical forcing, and secondary circulations associated with upper-level jet streaks contribute to MPS development.

CSI was evaluated by diagnosing regions where the equivalent potential vorticity is negative in a convectively stable atmosphere. A Colorado snowstorm

provided an example of CSI with banded precipitation oriented parallel to the mid-tropospheric thickness. The Minnesota Halloween storm that produced over three feet of snow in eastern Minnesota revealed that precipitation was enhanced by a frontogenetical circulation associated with a north-south oriented warm front. The importance of secondary ageostrophic circulations associated with the entrance and exit regions of upper-level jet streaks is illustrated by the 27-28 December 1990 and 20-22 April 1992 storms. Diagnoses of the December 1987 "bomb" case revealed that elevated convective instability associated with a well defined warm front and system-relative isentropic upward motions produced heavy narrow snow bands.

These case studies are used to highlight those physical processes which organized frozen precipitation events in the winter season over mesoscale regions. These processes should be of interest to forecasters to not only diagnose these events, but to more carefully interpret numerical model forecasts viewed through PC-GRIDDS.

MESOSCALE PRECIPITATION SYSTEMS IN WINTER STORMS

Mark Arthur Kaster, B.S.

A Thesis Presented to the Faculty of the Graduate School of Saint Louis University in Partial Fulfillment of the Requirements for the Degree of Master of Science (Research)

1993

COMMITTEE IN CHARGE OF CANDIDACY:

Professor James T. Moore,
Chairperson and Advisor

Professor Gandikota V. Rao

Assistant Professor Charles E. Graves

ACKNOWLEDGMENTS

I would like to express my deepest appreciation to my friend and advisor, Dr. James T. Moore, for his inspiration, guidance, and encouragement throughout the completion of this thesis. I would also like to thank the members of my research committee, Dr. Gandikota V. Rao and Dr. Charles E. Graves, for their assistance. A special thanks to fellow students: Rob, Chuck, Marty, Andrea, Sepi, Sean, and Kadir for all their encouragement. Thanks also to Mark Clausen and Mike Crowder for their support. I also thank the United States Air Force for the opportunity to undertake this research.

Some other special people deserve my unending thanks as well. To my parents, Arthur and Beverly, for providing me with the home, education, and support that has taken me to this point. To my young daughters, Amanda and Abby, whose constant smiles, hugs, and love make this work worthwhile and life very enjoyable. Finally, and most importantly, to my wife, Tracy, whose endless patience, encouragement, and love enabled me to complete the master's program. Our special "never-ending story" continues.

TABLE OF CONTENTS

LIST OF FIGURES

1. INTRODUCTION

Heavy frozen precipitation (usually snow) produced by complex mesoscale structures embedded within winter extratropical cyclones affects many areas of the United States each year. These precipitation events significantly affect agriculture, transportation, and utility industries, and almost every facet of life in the midlatitude winter season. Heavy local snowfalls affect the hydrology of large areas due to substantial augmentation to the existing snowpack. Also, tourism enjoys the benefits of good skiing conditions after a locally heavy snowfall occurs.

Major frozen precipitation events can and have paralyzed many regions of the United States, including large urban areas. For example, between 31 October and 2 November 1991, a strong winter extratropical cyclone (ETC) produced an extensive area of heavy snowfall and ice > 30 cm (> 12 in) from Iowa through Minnesota and Wisconsin into southern Canada. Total snowfall accumulation was over 91.4 cm (36 in) between Minneapolis/St. Paul and Duluth, Minnesota. The storm paralyzed much of the eastern half of Minnesota for many days. Storm Data (1991 b,c) reported that at least 20,000 homes experienced power outages. Many

rural areas were without power for a week. Over 900 schools and businesses were closed on 1 November. The storm closed many primary and secondary roads around Minneapolis/St. Paul for several days and shut down operations at Minneapolis International Airport for many hours. The governor of Iowa declared 52 of 99 counties in Iowa disaster areas because of the severity of this storm. In Iowa over 80,000 homes experienced power outages. Significant damage occurred to the states corn crop. The storm was considered the most costly in Iowa history (Storm Data 1991b). This is one example of the impact heavy frozen precipitation produced by complex mesoscale structures embedded within winter ETCs can have on an area.

1.1 Scientific Problem

The initiation, organization, and movement of mesoscale precipitation systems (MPSs) associated with winter ETCs must be better understood to accurately forecast their effects. Forecasting the development and movement of winter MPSs is a difficult problem for operational meteorologists. The environmental forces that play a role in MPS development occur mostly within the mesoscale while the forecaster is constrained to using largely synoptic data to attempt to resolve the

MPS. This forces the operational and research meteorologist to develop forecast techniques from synoptic scale datasets which help to isolate likely regions of mesoscale development.

Heavy frozen precipitation events may be associated with several forcing mechanisms. The scientific problem addressed in this thesis is to develop techniques to diagnose those physical processes leading to MPS development in the hope that the operational meteorologist may apply them directly to winter storms. These diagnostic tools, based on synoptic scale datasets, will resolve those forcing mechanisms responsible for MPS events within larger scale precipitation regimes. The following forcing mechanisms are explored:

1) System-relative (S-R) isentropic vertical velocities and streamlines
2) Conditional symmetric instability (CSI)
3) Elevated convection
4) Frontogenetical forcing
5) Upper-level jet (ULJ) secondary ageostrophic circulations.

1.2 Research Objective

The goal of diagnosing mesoscale forcing surrounded by synoptic or macro β scale features is fulfilled through a comprehensive study of several winter storms exhibiting mesoscale precipitation patterns. Each case will be examined using constant pressure and isentropic datasets to isolate the possible contributing factors to heavy precipitation. An objective of this research is to ascertain the role of the above mentioned mesoscale forcing in the initiation and development of MPSs that are organized within macro β scale features of the ETCs.

2. BACKGROUND LITERATURE

Over the last two decades researchers have found that precipitation in ETCs tends to be concentrated within mesoscale areas. These mesoscale areas have horizontal dimensions of tens to hundreds of kilometers. The larger mesoscale areas tend to be elongated with lengths exceeding widths by a factor of 2 or more. Palmen and Newton (1969) discussed the early research of mesoscale precipitation areas. Houze et al. (1976), Hobbs (1978), and Matejka et al. (1980) have categorized five types of mesoscale precipitation bands (see Fig. 1 for relationship of bands to the cyclone). The precipitation bands include:

1. Warm frontal bands (1a/1b): These bands are typically about 50 km wide and are oriented parallel to the surface warm front. They may be subdivided into two types. Type 1a bands are situated ahead of the surface warm frontal zone. Type 1b are associated with the surface warm frontal zone.

2. Warm sector bands (2): These bands are found in the warm sector of the cyclone, are typically 50 km wide, and are oriented parallel to the surface cold front.

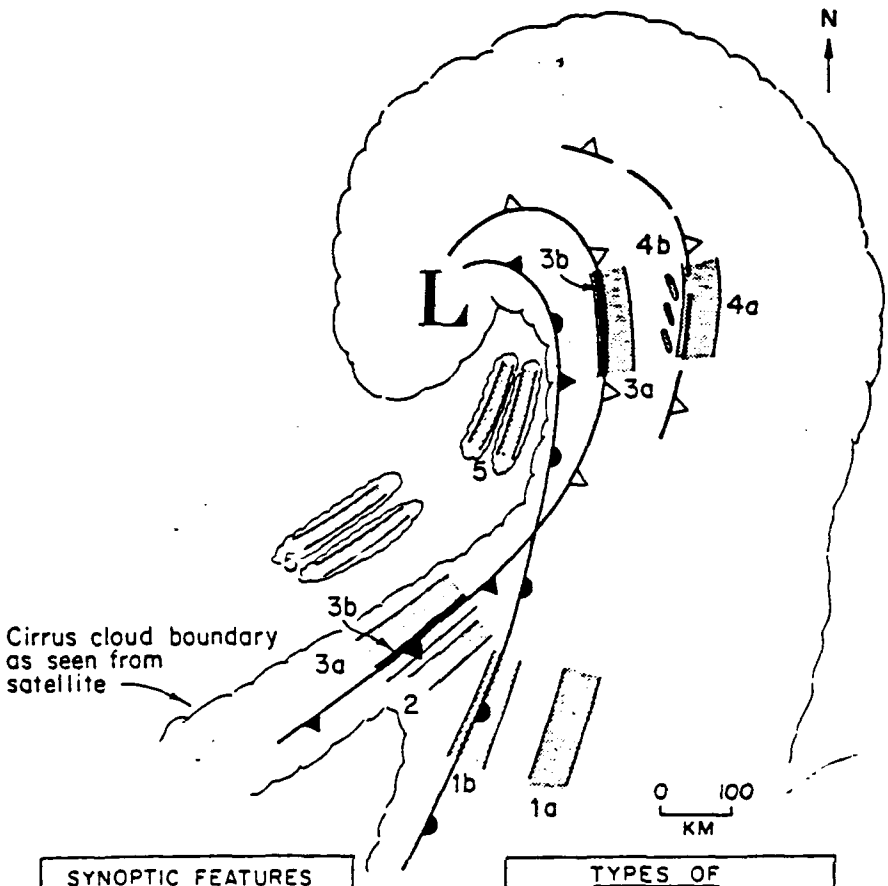

SYNOPTIC FEATURES	
L	SURFACE LOW-PRESSURE CENTER
	SURFACE COLD FRONT
	SURFACE WARM FRONT
	SURFACE WARM OCCLUDED FRONT
	COLD FRONT ALOFT
	PREFRONTAL COLD SURGE ALOFT

TYPES OF MESOSCALE RAINBANDS	
1.	WARM-FRONTAL
2.	WARM-SECTOR
3a.	WIDE COLD-FRONTAL
3b.	NARROW COLD-FRONTAL
4.	PREFRONTAL COLD-SURGE
5.	POSTFRONTAL

Fig. 1 Schematic representation of the types of rainbands (stippled areas) observed in cyclonic storms (see text for details). (Hobbs 1978)

3. Cold frontal bands (3a/3b): These bands are parallel to the cold front and may be subdivided into two types. Type 3a bands are wide (about 50 km) and tend to straddle (or are behind) the surface cold front. In the case of occlusions, they are associated with the cold front aloft. Type 3b cold frontal bands are quite narrow (about 5 km) and coincide with the leading edge of the surface cold front or cold front aloft.

4. Prefrontal, cold surge bands (4a/4b): These bands are associated with the surge of cold air ahead of the primary cold front found in an occlusion. They may be subdivided into two types. Type 4a bands are about 50 km wide and straddle the leading edge of the prefrontal cold surge aloft. Type 4b bands are a series of wave-like bands situated within the prefrontal cold surge aloft. Houze et al. (1976) called the latter features wave bands since they occur in a very regular pattern, similar to waves, and are typically 10-20 km wide.

5. Post frontal bands (5): These bands may occur in several lines within one cyclone and form well behind and parallel to the cold front and occlusion in the cold air. They are within the convective cloud field behind the frontal cloud shield.

2.1 Isentropic System-Relative Vertical Motion and Streamlines

Isentropic analysis is used to gain a better representation of vertical motions in the atmosphere. The advantages of using isentropic analysis in analyzing atmospheric flow have been discussed by many researchers (Saucier 1955; Uccellini 1976; Moore 1992). Some advantages of using an isentropic surface over a pressure surface are (Moore 1992):

1) Air parcels are thermodynamically bound to their isentropic surface in the absence of diabatic processes.

2) Flow along an isentropic surface contains the adiabatic component of vertical motion, neglected on a constant height or pressure surface.

3) Isentropic surfaces tend to better represent the true moisture pattern in space-time than moisture transport on standard 850 mb or 700 mb charts. As Moore points out, this advantage is probably one of the greatest of isentropic analysis. Many forecasters have seen patches of moisture "pop up" on 850 mb or 700 mb charts, especially during warm air advection (overrunning) situations. This moisture is coming up from below the 850 mb or 700 mb surfaces -- a process viewed more coherently on an isentropic surface.

4) Frontal discontinuities occur more readily on constant pressure surfaces than on isentropic surfaces. Constant pressure surfaces cut through frontal zones causing frontal zone quantities to change radically over subsynoptic scales. Isentropic surfaces run parallel to the frontal zone causing wind, moisture, temperature, etc., to change gradually, i.e., more realistically. This property makes isentropic analysis extremely useful in diagnosing kinematic and dynamic variables in baroclinic zones.

5) The vertical separation between isentropic surfaces is a measure of static stability. This separation indicates strong (weak) static stability when isentropic surfaces are close together (far apart).

6) The slope of an isentropic surface in the vertical is directly related to the thermal wind. A vertically sloping isentropic surface is indicative of a strong thermal contrast. This is represented on the isentropic surface as a tight packing of isobars or isotherms. An isentropic surface that tilts up or down can indicate a frontal zone and a change in wind velocity with height.

Vertical motion can be computed on isentropic surfaces because the horizontal flow along isentropic surfaces contains the adiabatic component of vertical

motion (Moore 1992). Adiabatic vertical motion can be defined as:

$$\omega = \mathbf{V} \bullet \nabla P \qquad (1)$$

Saucier (1955) notes that it is important to account for the horizontal motion of the isentropic surface. If **C** represents the velocity of the system, then the system-relative (S-R) vertical motion can be written as (Moore 1992):

$$\omega = (\mathbf{V} - \mathbf{C}) \bullet \nabla P \qquad (2)$$

V - **C** measures the relative motion toward lower isentropic pressures (upslope flow) or higher isentropic pressures (downslope flow). Typically $|\mathbf{V}| > |\mathbf{C}|$, meaning the isentropic surface is being displaced horizontally more slowly than the air. (2) expresses S-R adiabatic vertical motion. Negative (positive) values imply upward (downward) motion on an isentropic surface.

S-R streamlines can be excellent for displaying regions of confluence/diffluence, which, in an isentropic framework, can be associated with destabilization/stabilization (Moore 1992). Streamlines crossing isobars generally imply vertical

motion. S-R streamlines are identical to trajectories relative to the moving system (Carlson 1991).

2.2 Conditional Symmetric Instability

Conditional symmetric instability (CSI) is an important property of the atmosphere when diagnosing and predicting mesoscale bands of moderate to heavy precipitation within winter ETCs. Research has shown that within regions of CSI slantwise convection can increase snow totals over meso β scale (20 - 200 km) regions. CSI has been discussed by Bennetts and Hoskins (1979), Emanuel (1983, 1985, and 1988), Sanders and Bosart (1985), Snook (1992), and Moore and Lambert (1993). The importance of CSI in winter storms in creating mesoscale precipitation bands has been documented by Sanders and Bosart (1985), Sanders (1986), and Moore and Blakely (1988). Bennetts and Hoskins (1979), Emanuel (1983), Martin et al. (1992), and Shields et al. (1991) show that CSI can be diagnosed by computing equivalent potential vorticity (EPV). However, recently Moore and Lambert (1993) explicitly showed the relationship between CSI and EPV. The present research is based on Moore and Lambert's technique of computing EPV and evaluating CSI, and

distinguishing regions of CSI from those of upright convection.

Symmetric instability is the result of a combination of horizontal (inertial versus centrifugal) and vertical (buoyancy versus gravitational) forces. Although the atmosphere may be stable to both purely vertical and purely horizontal motions, it may be unstable to certain slantwise motions. Lilly (1986) shows that the process of evaluating CSI involves the determination of both inertial (horizontal) and buoyant (vertical) stability of the parcel.

Absolute geostrophic momentum (*Mg*) is used to evaluate the inertial stability of a parcel. Emanuel (1983) defines Mg in a steady, geostrophic balanced flow as:

$$Mg = Vg + fx \qquad (3)$$

where Vg is the environmental wind normal to the cross-sectional plane, f is the Coriolis parameter, and x is the distance along the x-axis (normal to Vg).

CSI can be evaluated in a near-saturated environment (RH > 80%, Bennetts and Sharp 1982) by

taking a cross section normal to the mid-tropospheric thermal wind and displaying lines of constant Mg and θe, the equivalent potential temperature (Moore and Blakely 1988). CSI is found in those regions where Mg surfaces are "flatter" (more horizontal) than the θe surface. Bluestein's (1986) research indicates CSI is found when large vertical wind shear, large anticyclonic wind shear, and low static stability occur. Mg surfaces will be relatively horizontal when Vg increases with height as found in areas of large vertical wind shear. Absolute vorticity approaches zero when anticyclonic wind shear is present, creating a weak stable zone. This may contribute to CSI. In low static stability regions, isentropic and θe surfaces will be close to vertical, possibly contributing to CSI.

Martin et al. (1992) evaluated CSI by computing the equivalent potential vorticity (EPV) as:

$$EPV = -\eta \bullet \nabla \theta e \qquad (4)$$

where η is the three-dimensional absolute vorticity vector, ∇ is the three-dimensional del operator in x, y, p coordinates. Neglecting Y - variations and terms with ω (vertical motion in pressure coordinates), assuming geostrophic flow, multiplying by g

(gravitational acceleration), and using Mg as defined previously, (4) becomes:

$$EPV = g((\partial Mg/\partial p \; \partial \theta e/\partial x) - (\partial Mg/\partial x \; \partial \theta e/\partial p)) \quad (5)$$

EPV can be used as a diagnostic tool to analyze areas of CSI. Areas where EPV is less than 0 in a convectively stable environment indicate areas of CSI, areas of EPV greater than 0 indicate areas of conditional symmetric stability (CSS).

2.3 Elevated Convection

Although some work on elevated convection in warm season convective systems has been done, relatively little research has applied this forcing mechanism to winter storms. Elevated convection is defined as convection isolated from surface diabatic effects by a frontal inversion (Colman 1990a, 1990b). This structure differs from cumulus convection in which surface sensible and latent heat forces in the planetary boundary layer contribute to the destabilization of the atmospheric column. Kocin et al. (1985) used the Mesoscale Atmospheric Simulation System (MASS) to simulate dynamical interactions and diabatic processes for an intense convective snowburst

along the East Coast. Elkins (1987) did a comprehensive empirical study of thunderstorms with snow. He documented the synoptic-climatology of "thundersnow" occurrences and examined the development of cyclones producing convective snow events. Scofield and Robinson's (1990) work focused on using instability bursts and satellite imagery to analyze and NOWCAST heavy snow. Instability bursts are defined as a thrust of maximum atmospheric destabilization into an area. They illustrated the use of θe advection (i.e., overrunning) and satellite imagery for analyzing heavy snow events. In the satellite imagery, instability bursts are identified as developing subsynoptic scale wave patterns, baroclinic leaf-type patterns, or convective cloud areas or bands embedded within the ETC cloud pattern. Heavy snow from elevated convection was observed to occur in the gradient region of strong θe advection.

Recently, Colman (1990a, 1990b) studied thunderstorms that occur above frontal surfaces. From his work it appears that elevated thunderstorms display characteristics different from summer-season surface-based convection, most notable being the tendency to occur in environments without positive convective available potential energy (CAPE). Once the thunderstorms became elevated above the frontal surface, the convective instability quickly diminished.

These thunderstorms were seen to continue for many hours and to develop in the stable environment above the front. He believes elevated convection takes place in two steps. Initially, high θe air overlying the front is stable to vertical displacements, but inertially unstable. Then, along the instantaneous path of the unstable parcel, the thermodynamic structure changes, the parcel becomes gravitationally unstable, and upright convection results. The work in this thesis is an extension of Colman's research, but focuses entirely on elevated convection in winter storms.

Carlson (1980, 1991) and Browning (1986) developed conceptual models of airflow through midlatitude cyclones to improve on the frontal models of the Norwegian school. The result of their work is the conveyor belt theory which identifies the major cloud and precipitation producing flow in a S-R frame of reference. The conveyor belt theory also provides the operational and research meteorologist with a better conceptional model of where and when elevated convection may form in winter ETCs.

In Carlson's (1980, 1991) and Browning's (1986) conceptual models, frontal zones arise from the confluence of airstreams with differing properties and

origins. In the lower troposphere, the cold front represents a boundary between the warm conveyor belt (WCB) and the dry airstream from the upper levels west of the trough. The warm front is the boundary between the WCB and the cold conveyor belt (CCB) originating from the east-northeast. Upper-level frontal zones and jet streams are associated with the confluence between airstreams that produce sharp boundaries in the cloud pattern along the west edge of the comma cloud tail as well as the edge of the anticyclonically curved cirrus shield northeast of the flow.

Figure 2 shows airflow in which the WCB undergoes forward slope ascent ahead of a kata cold front before rising above a flow of cold air ahead of a warm front. Cold middle-tropospheric air with low θw (or θe) overruns the cold front and generates convective instability in the upper portions of the WCB. Elevated convection may occur ahead of the warm front in the upper portions of the WCB.

Figure 3 shows the WCB undergoing forward slope ascent similar to Fig. 2, but with the leading edge of the overrunning dry, low θw air advancing ahead of the surface cold front, producing a well-defined upper cold front. Elevated convection may occur with the cells associated with the upper cold front.

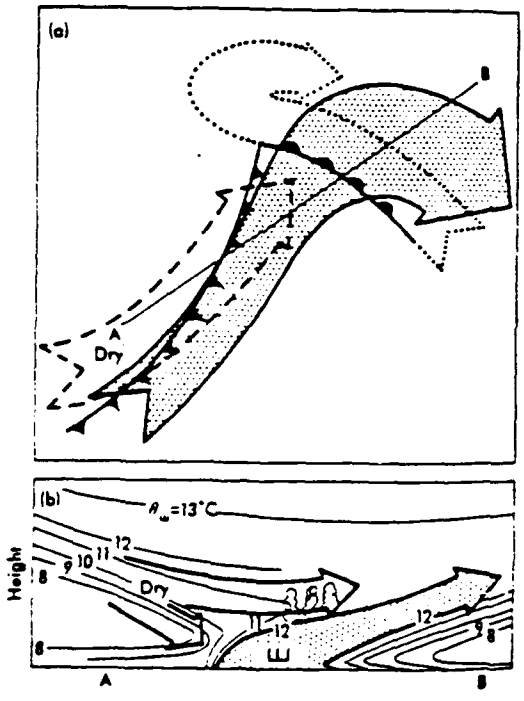

Fig. 2 Schematic portrayal of airflow in a midlatitude cyclone in which the warm conveyor belt (solid arrow with stippled shading) is undergoing forward-sloping ascent ahead of a kata cold front before rising above a flow of cold air ahead of the warm front - the cold conveyor belt. Cold middle tropospheric air with low θw (dashed arrow) is shown overrunning the cold front and generating potential instability in the upper portions of the warm conveyor belt. Plan view and vertical section as shown in (a) and (b). The section in (b) is along the line AB in (a).
(Browning 1986)

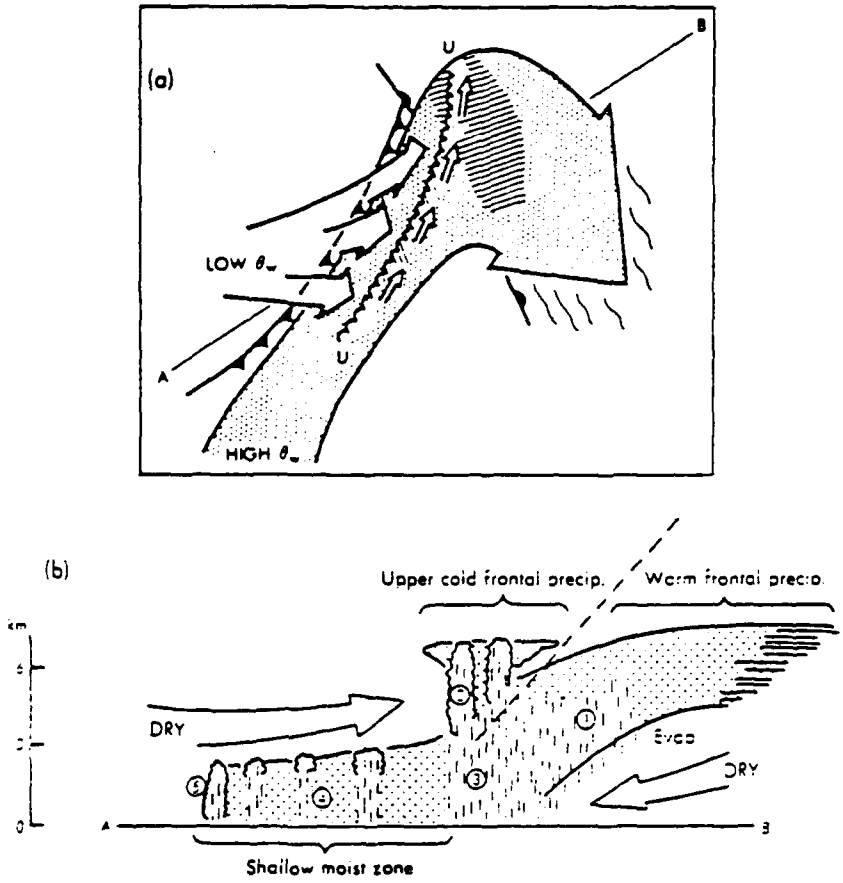

Fig. 3 Schematic portrayal of the same situation as in Fig. 2 with the warm conveyor belt undergoing forward-sloping ascent but drawing attention to the split-front characteristic and the overall precipitation distribution. (a) is plan view, (b) is the vertical section along AB in (a). In (a) UU represents the upper cold front. Numbers in (b) represent precipitation type: 1) warm frontal precipitation, 2) convective precipitation-generating cells associated with the upper cold front, 3) precipitation from the upper cold frontal convection descending through an area of warm advection, 4) shallow moist zone between the upper and surface cold fronts, 5) shallow precipitation at the surface cold front.
(Browning 1986)

2.4 Frontogenetical Forcing

Moore and Blakely (1988), Sanders and Bosart (1985), Emanuel (1985), and Shields et al. (1991) have shown that frontogenetical forcing may be the mechanism for some heavy banded precipitation structures formed in MPS events. Sanders and Bosart's research show that large scale geostrophic confluence acts to increase the horizontal temperature gradient by horizontal advection, and to decrease the vertical wind shear by horizontal momentum advection, upsetting the thermal wind balance. A thermally direct transverse circulation is induced to restore this balance (see Fig. 4a). Emanuel (1985) has shown that if potential vorticity vanishes in the warm air sector the ascent in the warm air becomes intense and concentrated (see Fig. 4b). The downdraft is not enhanced in the cold air. Since upward and downward mass fluxes must balance, the updraft must be horizontally restricted; producing the possibility of mesoscale banded precipitation (Sanders and Bosart 1985). In other words, frontogenesis in a symmetrically neutral base state may occur with the upward branch of a frontal circulation considerably enhanced by low potential vorticity.

Shields et al. (1991) studied the dynamical forcing and mesoscale organization of banded precipitation

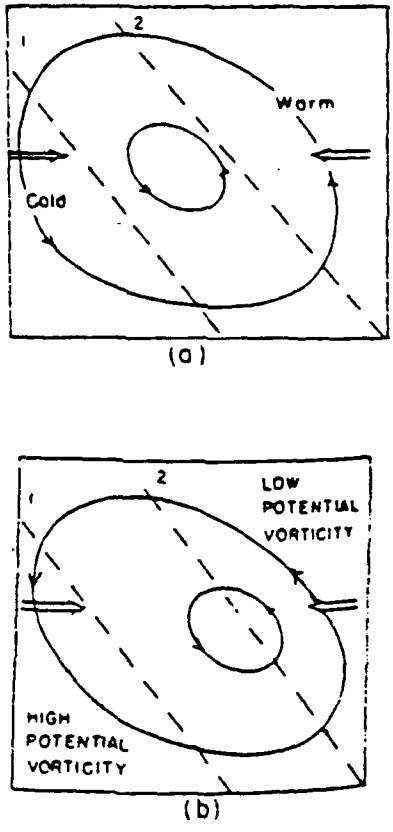

Fig. 4 Vertical cross section of idealized transverse circulations accompanying large-scale frontogenetical confluence (double-shafted arrows): (a) uniform potential vorticity and (b) vanishing potential vorticity in warmer air. Dashed lines are potential isotherms. (Sanders and Bosart 1985)

embedded in a winter storm over the Midwest. As part of their research they examined in detail the evolution of the surface flow fields and frontogenetical forcing as mechanisms in the band formation. Three precipitation band types were found in the storm -- the strongest and widest band occurred in a strongly frontogenetic environment. The axis of maximum frontogenetic forcing and the band formed by frontogenetic forcing was found parallel to the thermal wind field.

2.5 Upper Level Jet Secondary Ageostrophic Circulation

There is increasing evidence for the important role of a dual jet streak pattern in locally enhancing the vertical motion, precipitation rates, and the development rates associated with ETCs. Hakim and Uccellini (1992) diagnosed coupled jet streak circulations based on a numerical simulation from the operational nested-grid model (NGM). Their research reveals that large values of upper-tropospheric ascent correspond to the time interval when the anticyclonic entrance of one jet streak located to the north of the cyclone and the cyclonic exit of the jet streak located to the south of the storm are in close proximity. They use the NGM data to show how it is possible for

transverse circulations associated with separate jet streaks to merge to focus a region of ascent that contributes to the rapid development of a narrow snow band.

Funk (1991) shows there is increasing acceptance by forecasters of the importance of jet streak circulation patterns in contributing to heavy precipitation events. He reviews the forecasting techniques employed in the Forecast Branch of the National Meteorological Center (NMC) and cites the role of the dual-jet pattern in focusing heavy precipitation. Figure 5 shows the three-dimensional schematic of jet streak circulation patterns during East Coast snowstorms based on Uccellini and Kocin (1987).

The above forcing mechanisms will be studied and applied to several winter storm cases where MPSs developed. Each case will be researched to understand which forcing mechanism is responsible for the development of the MPS within a large scale precipitation region.

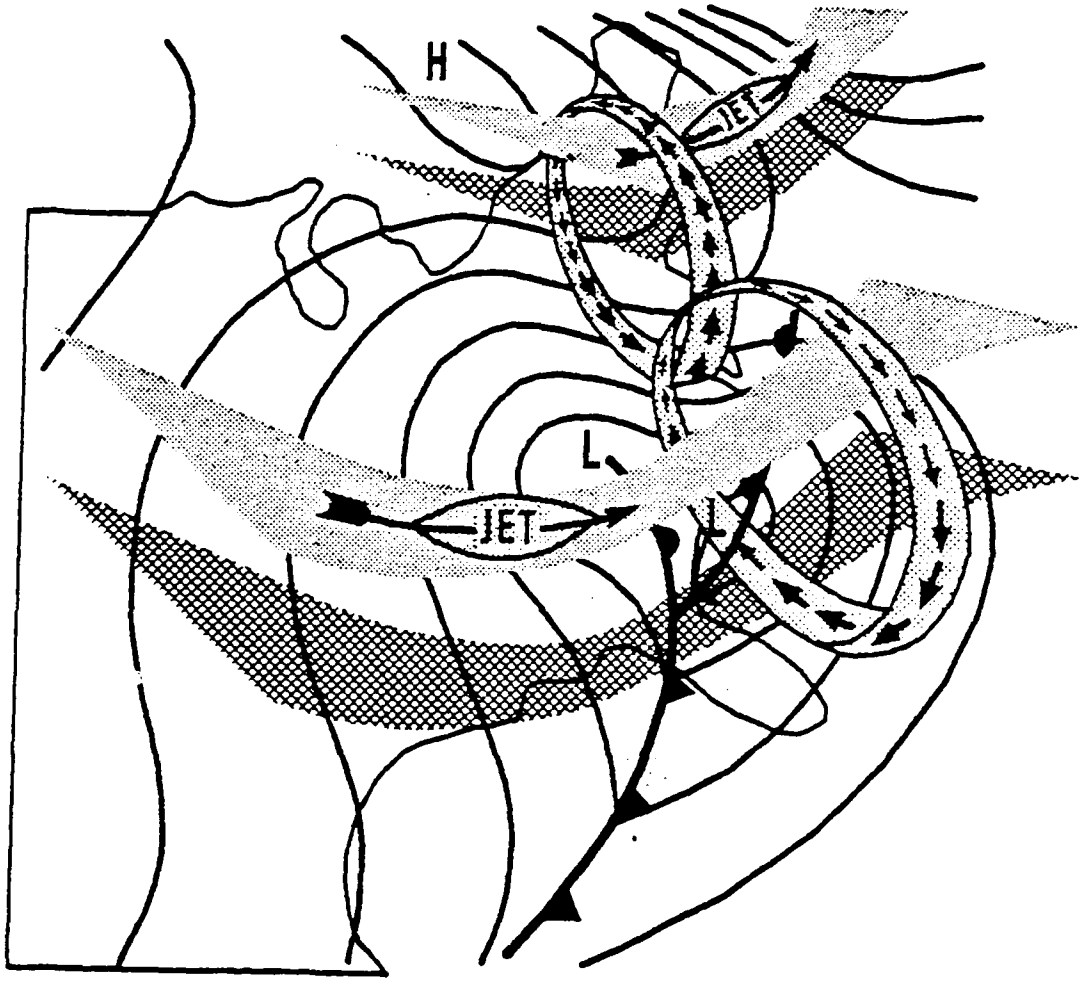

Fig. 5 Three-dimensional schematic of jet-streak circulation patterns during East Coast snowstorms.
(Uccellini and Kocin 1987)

3. METHODS AND PROCEDURES

The objective of this thesis was accomplished through the collection and processing of upper air and surface data from the United States, Canada, and Northern Mexico. The raw data were objectively analyzed to produce gridded data fields on constant pressure and isentropic surfaces. The analyzed data were used to calculate isentropic S-R vertical motion and streamlines, ageostrophic winds, kinematic omegas, CSI/EPV, frontogenesis, vertical wind shear, and secondary ageostrophic vertical circulations over the areas of interest. These diagnostic fields were used to diagnose which of the forcing mechanisms occurred to produce the heavy precipitation. Completion of the entire methodology for several cases achieved the research objective which was to develop diagnostic techniques from synoptic scale datasets that help isolate those forcing mechanisms responsible for MPS development within winter ETCs.

The cases researched included:

CASE	DATES OF STORM
1) Colorado Banded Snow Case	1/19/91 - 1/20/91
2) Minnesota Snow Case	10/31/91 - 11/02/91

3) Eastern Missouri Snow Case 12/27/90 - 12/28/90

4) Eastern Kansas - Nebraska Snow Case 4/20/92 - 4/22/92

5) Central US Snow Case 12/13/87 - 12/16/87

3.1 Data Sets

Data from the standard rawinsonde network and surface observation stations were archived from the Domestic Data Service Plus (DDS+). Upper air data from nearly 100 stations were collected every 12 hours with an average station spacing of 400 km. Height, temperature, dewpoint temperature, and wind data were extracted at 50 mb intervals from 900 - 100 mb to create objectively analyzed fields. This raw data was used to create soundings at each station. The soundings were used to diagnose areas of stability and the vertical wind profile. Pressure data were converted to isentropic coordinates using the Duquet (1964) isentropic program. Soundings were vertically interpolated to potential temperature levels from 270 K to 370 K with a 2 K interval.

The surface data for approximately 620 stations were collected every hour with an average station spacing of 150 km. Temperature, dewpoint temperature,

pressure, and wind components were used to create objectively analyzed fields using the Barnes (1973) objective analysis scheme described below.

The upper air and surface data for each case were checked for errors and missing data. Errors found in the data were corrected; data was obtained and added if found to be missing. No gross errors were detected. The objective analysis and smoothing procedures (e.g. Barnes 1973; O'Brien 1970) reduce the effects of data errors; however, they do not remove them.

Satellite imagery was saved from the PC-McIDAS circuit or downloaded from the University of Wisconsin Space Sciences and Engineering Center. PC-McIDAS software (from UNIDATA) was used to gather, examine, and archive the satellite imagery. Infrared imagery was collected at 1 hour intervals. The GOES MB enhancement curve was used to identify the strongest convective elements (-55 to -62 C) and to track storm movement. A winter enhancement curve was developed to resolve the enhanced cloud bands located in the lower, warmer regions of the cloud field. This was accomplished by creating an enhancement pallet in the -27 to -50 C temperature range. Loops were built and centered at the 00 UTC and 12 UTC times in order to take advantage of the availability of large datasets.

3.2 Objective Analysis

Objectively analyzed fields for upper air and surface data were generated using the Barnes (1973) technique. Upper air objectively analyzed fields of wind, temperature, dewpoint temperature, potential temperature, and equivalent potential temperature were interpolated to a 31 x 23 grid with a 190.5 km grid spacing at 17 levels from 900 to 100 mb. The Barnes parameters of c = 81900 km^2 and gamma = 0.20 were used to resolve 37% of the 2-delta waves of 800 km. Surface objectively analyzed fields of wind, temperature, dewpoint temperature, and potential temperature were interpolated to a 53 x 35 grid with a 95.25 km grid spacing. At the surface Barnes parameters of c = 22000 km^2 and gamma = 0.40 were used to resolve 27% of the 2-delta waves of 500 km.

3.3 Computational Procedures

3.3.1 Isentropic System-Relative Vertical Motion and Streamlines

As stated in section 2.1, vertical motion can be computed on isentropic surfaces. In this research the horizontal motion of the isentropic surface is taken

into account. C represents the velocity of the system in the S-R omega equation, (2) (Moore 1992).

An estimate of C was computed by calculating the 12 hour movement of the respective ETC's absolute vorticity maximum. It is important to note that since all grid points on a US map will use this C value, areas distant from the influence of the vorticity maximum may not yield accurate results since their vertical motions should be referenced with respect to a different, perhaps approaching/departing system.

S-R streamlines were calculated using the 12 hour movement of the pertinent absolute vorticity maximum, described earlier. S-R streamlines were then computed using $u - C_x$ and $v - C_y$ at each subpoint where C_x and C_y are the systems' east-west and north-south movement, respectively.

3.3.2 Ageostrophic Winds

After the gridded fields were created, many kinematic fields were computed for each of the 17 levels. The geostrophic wind components used to create ageostrophic winds were computed using the equations:

$$u_g = -1/f \, \partial\Phi/\partial y \qquad (6)$$

$$v_g = 1/f \, \partial\Phi/\partial x \qquad (7)$$

where Φ is the geopotential and f is the Coriolis parameter. The ageostrophic winds were computed as the difference between the real wind and the geostrophic wind.

3.3.3 Kinematic Omegas

Vertical motion was also computed on pressure surfaces using the kinematic method of computing omegas. This method involves the integration of horizontal divergence in the vertical from the surface to 100 mb (Holton 1979). Divergence is given by:

$$\nabla \cdot \mathbf{V} = \partial u/\partial x + \partial v/\partial y \qquad (8),$$

where u and v are the two wind components of the observed wind. Using observed winds to calculate divergence can be a major disadvantage of the kinematic method. Small errors in the observed wind components can cause large errors in the horizontal divergence fields. These errors can accumulate in the vertical as the horizontal divergence is integrated. At the

surface omega is assumed to be zero. This is a reasonable assumption except in regions where there is considerable slope to the terrain or where the ageostrophic wind is significant (Holton 1979). The accumulation of wind errors created by vertically integrating divergence causes omega at 100 mb to rarely be zero. The O'Brien (1970) linear adjustment scheme was used to correct the errors (force omega at 100 mb to be zero) and adjust the vertical motion pattern at the boundaries of the atmosphere -- between the surface and 100 mb.

3.3.4 Conditional Symmetric Instability and Equivalent Potential Vorticity

As discussed in section 2.2, EPV can be used to diagnose areas of CSI. To compute EPV, Mg and θe were calculated. Mg and θe fields were generated using objectively analyzed fields of θe and the geostrophic wind components (u_g and v_g). As discussed above, EPV in this thesis is defined as (Martin et al. 1991; Moore and Lambert 1993):

$$EPV = g((\partial Mg/\partial p \; \partial \theta e/\partial x) - (\partial Mg/\partial x \; \partial \theta e/\partial p)) \qquad (9)$$

Term A Term B Term C Term D

Term 1 = Term A x Term B Term 2 = Term C x Term D

where g = 9.806 m s^{-2}. The equation is multiplied by g so that units of EPV will be the same as potential vorticity units (PVU) in SI notation, 1 PVU = 10^{-6} m^2 K s^{-1} kg^{-1}. Values of EPV < 0 in a convectively stable environment indicate CSI; EPV > 0 indicate CSS.

Moore and Lambert (1993) give a term by term explanation of (9) that helps explain the relationship between EPV and CSI. Term A represents the change in absolute geostrophic momentum with respect to pressure and is generally negative below the level of the jet stream. From (3), Mg is directly proportional to Vg. Under normal conditions Vg increases as pressure decreases up to the jet stream level. Term A will become smaller (more negative) and the slope of the Mg surfaces will decrease (Mg surfaces become more horizontal) as the vertical wind shear increases (because Vg increases with height).

Term B is generally positive because of Mg, which requires the cross section to be taken normal to the geostrophic wind. The result is that the cross section is also normal to the 850 - 300 mb thickness pattern or thermal wind. Since the positive x direction on each cross section points toward warmer air, equivalent potential temperature surfaces slope down, resulting in term B > 0. The net result of term A multiplied by

term B will be a negative number made more negative by a stronger horizontal θe gradient or vertical wind shear.

Term C is usually positive. Since Mg = Vg + fx, $\partial Mg/\partial x$ is the absolute vorticity (since Ug is 0). The absolute vorticity is usually > 0 in the northern hemisphere. An exception would result from a very strong decrease in Vg in the positive x direction. This may overpower the increase in Mg due to fx and cause term C to become negative. In most cases, the gradient of Vg in the x direction is not strong enough to cause term C to be < 0.

Term D is a measure of the convective stability of the atmosphere. If term D < 0, the atmosphere is convectively stable. If term D = 0, the atmosphere is convectively neutral, and if term D > 0, the atmosphere is convectively unstable.

Moore and Lambert (1993) discuss the effect term D has on the value of EPV for each of the above cases assuming term 1 (term A x term B) is negative and term C is positive; this is usually true. When term D < 0, the atmosphere is convectively stable, making term 2 negative. When term 2 is subtracted from term 1 in (9), the net result is an increase of EPV and decreased

chance for CSI. When term D = 0, the atmosphere is convectively neutral. This makes term 2 = 0; net result is term 2 doesn't affect the value of EPV. When term D > 0, the atmosphere is convectively unstable. In this case convective instability dominates, resulting in upright convection. The atmosphere can be unstable to CSI and convective instability (Bennetts and Sharp 1982), but convection dominates due to its faster growth rate. This forces the researcher to differentiate between frontal regions exhibiting CSI and convective instability.

To locate areas favorable to CSI and to discriminate between regions of CSI and convective instability, terms 1 and 2 were evaluated. A cross section normal to the thickness was taken over the area of interest. Term 1 tends to be negative. Areas of positive or near zero values from term 2 indicate the likely existence of CSI. However, areas of negative values indicate convective instability since term 2 is < 0 only in convectively unstable regions. As discussed above, in negative value regions, upright convection is favored over CSI. Finally, the total EPV field for the cross section is calculated and displayed. This composite of terms 1 and 2 show regions that favor elevated convection over CSI and vice versa.

3.3.5 Frontogenetical Forcing

In this thesis the role of frontogenetical forcing is explored through the upper-level two-dimensional frontogenesis as discussed by Moore and Blakely (1988). Early two-dimensional kinematic theories (Petterssen 1936) showed a front would form along the axis of dilation as a result of a deformative component of the horizontal motion. The two-dimensional, adiabatic form of Miller's (1948) frontogenesis equation in pressure coordinates was used to compute frontogenesis for the upper air. It can be written:

$$F = 1/|\nabla\theta| \; (\partial\theta/\partial x[-\partial u/\partial x \; \partial\theta/\partial x - \partial v/\partial x \; \partial\theta/\partial y] + \partial\theta/\partial y[-\partial u/\partial y \; \partial\theta/\partial x - \partial v/\partial y \; \partial\theta/\partial y] + \partial\theta/\partial P[-\partial\omega/\partial x \; \partial\theta/\partial x - \partial\omega/\partial y \; \partial\theta/\partial y])$$

(10)

The sum of the first two right-hand side terms represents the horizontal deformation contributing to frontogenesis. The contribution of differential vertical motion (twisting) to frontogenesis appears in the third bracketed term (Boyle and Bosart 1986).

3.3.6 Secondary Circulations

Cross sections of the tangential ageostrophic component of the wind and vertical motion were generated to detect thermal circulations associated with jet streaks. The cross section program uses the previously calculated ageostrophic winds and kinematic omegas to generate the cross section components. The program interpolates vertical motion and ageostrophic winds to the cross sectional plane. The u and v ageostrophic wind components are used to compute ageostrophic wind components tangent to the cross-sectional plane. The end product is a plot showing a combined vector whose horizontal component is equal to the tangential ageostrophic wind and whose vertical component is equal to the vertical motion. In this way secondary, ageostrophic transverse frontal or jet streak circulations may be diagnosed.

4. RESULTS

4.1 Case 1: 19-20 January 1991

4.1.1 Synoptic Overview

A shortwave trough and vorticity maximum developed over northern British Columbia on 18 January 1991 and moved south into the United States Rocky Mountain region during the next 2 days (Fig. 6). This trough and its associated vorticity maximum crossed Colorado from northwest to southeast between 0000 and 1200 UTC 20 January 1991.

At the surface on 19 January, a cold front stretched from a low in Ontario through Minnesota, South Dakota, Wyoming, and Idaho (not shown). During the next 12 hours on 19 January the cold front moved through Colorado. The cold air surge behind the front caused temperatures to drop more than 10^{o} C over eastern Colorado between 1800 and 0000 UTC on the 19th. The Denver, Colorado (DEN) sounding (Fig. 7) shows the depth of the cold air to be rather shallow (approximately 3.5 km MSL) with near-saturation up to approximately 400 mb. A surface low pressure center developed in the southeast corner of the state at 0800

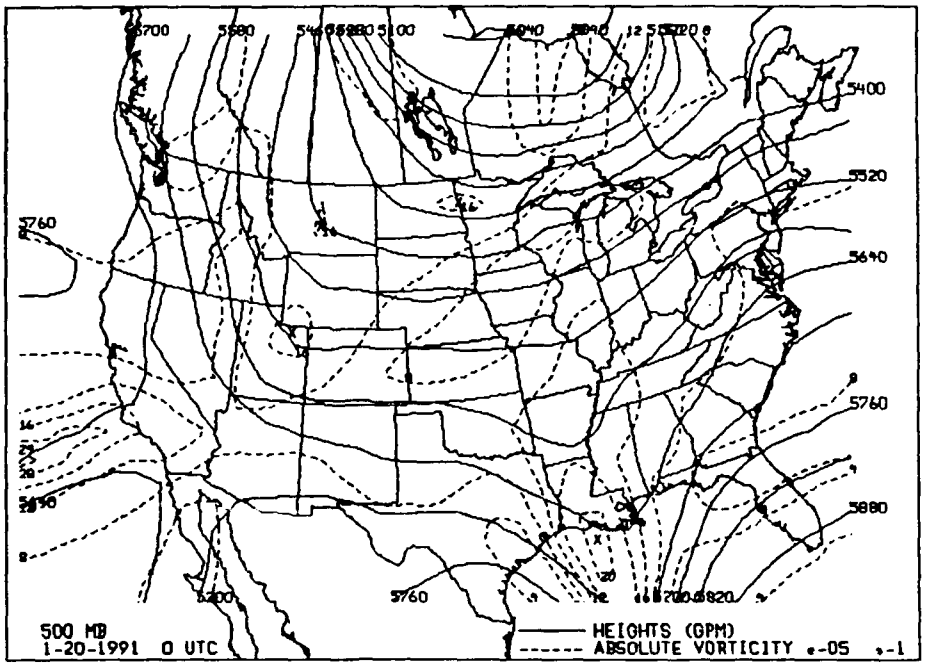

Fig. 6 500 mb chart with surface frontal position for 0000 UTC 20 January 1991. Height (solid lines)in geopotential meters (gpm) and absolute vorticity (dashed lines)(x 10^{-5} s^{-1}). X's mark vorticity centers.

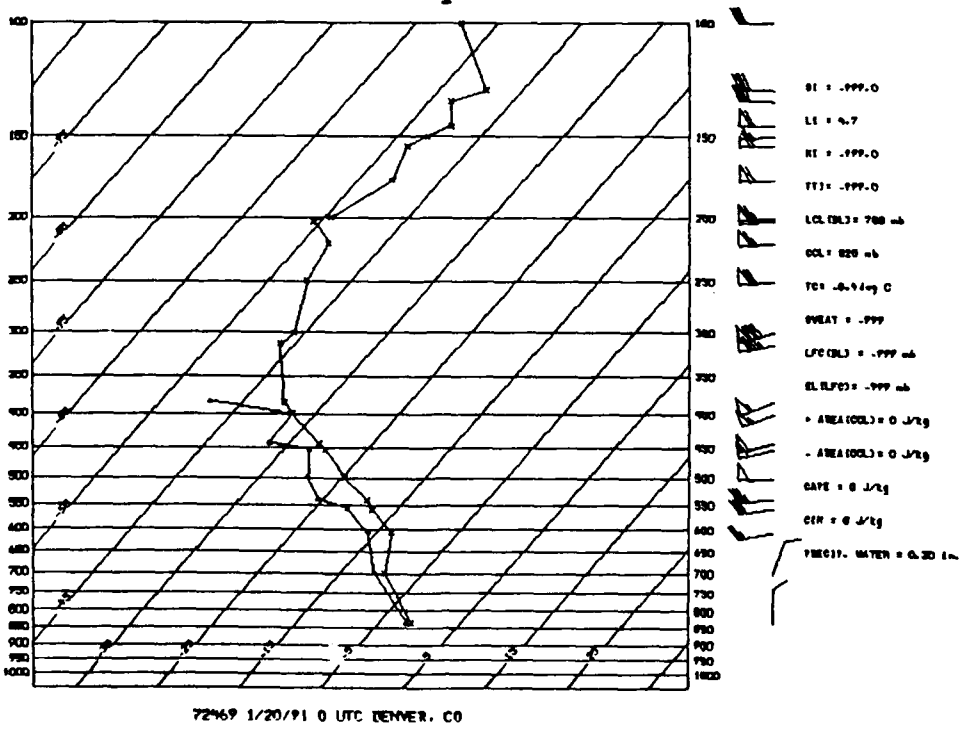

Fig. 7 Denver, Colorado sounding for 0000 UTC 20 January 1991.

UTC on the 20th and moved southeast during the next 12 hours.

This combination of synoptic features led to northeasterly, upslope surface winds in the Denver area. Snow began falling around 1800 UTC and lasted approximately 18 hours. Snow depths ranged between 2.5 to over 12 cm (1 - 5 in; Storm Data 1991a). The Mile-High Doppler Radar at Denver's Stapleton Airport, Colorado at 2300 UTC 19 January reported well-defined precipitation bands with reflectivities up to 32 dBZ (Fig. 8)

4.1.2 Isentropic Vertical Motion and Streamlines

To obtain an accurate representation of the atmospheric motion, an isentropic surface in the region of greatest baroclinicity was selected. The 292 K isentropic surface was used for this case.

Examining the lifted condensation pressure (LCP) (the level a parcel would need to rise to become saturated) data (not shown) for 0000 UTC 20 January on the 292 K isentropic surface revealed a broad area of moist air advecting north into Colorado from Texas.

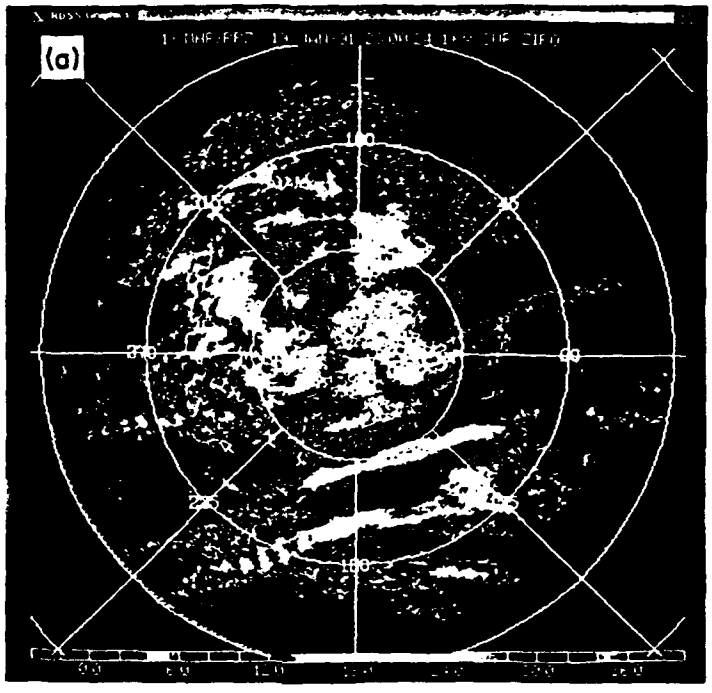

Fig. 8 Plan Position Indicator (PPI) at 1.6° elevation angle from Mile-High Radar 2300 UTC 19 January 1991. Reflectivity (color scale, in dBZ, is indicated by the color bar along the bottom of figure). Range rings are at 50 km. (Rasmussen et al. 1992).

Inspection of the LCPs reveals that the air would need to rise to 700 mb to reach saturation over southern and eastern Colorado.

Figures 9 and 10 show the ground relative (G-R) and S-R vertical motion for 0000 UTC 20 January. The G-R vertical motion values over Colorado are positive, indicating downward vertical motion (DVM) over the snow area. However, the S-R vertical motion values are much stronger. These S-R values show a much larger area of upward vertical motion (UVM) on the south side of the trough. The UVM over Colorado provided the large scale lifting within which the MPS (in this case banded precipitation) formed.

Figures 11 and 12 show the G-R streamlines and S-R streamlines for 0000 UTC 20 January. G-R streamlines display the inflow for the system from the north with air sinking from 650 mb to 850 mb over Colorado. The S-R streamlines are considerably different. They reveal a southeasterly inflow with the air rising to 700 mb over Colorado, the same level as the lifted condensation pressure data indicated saturation would occur.

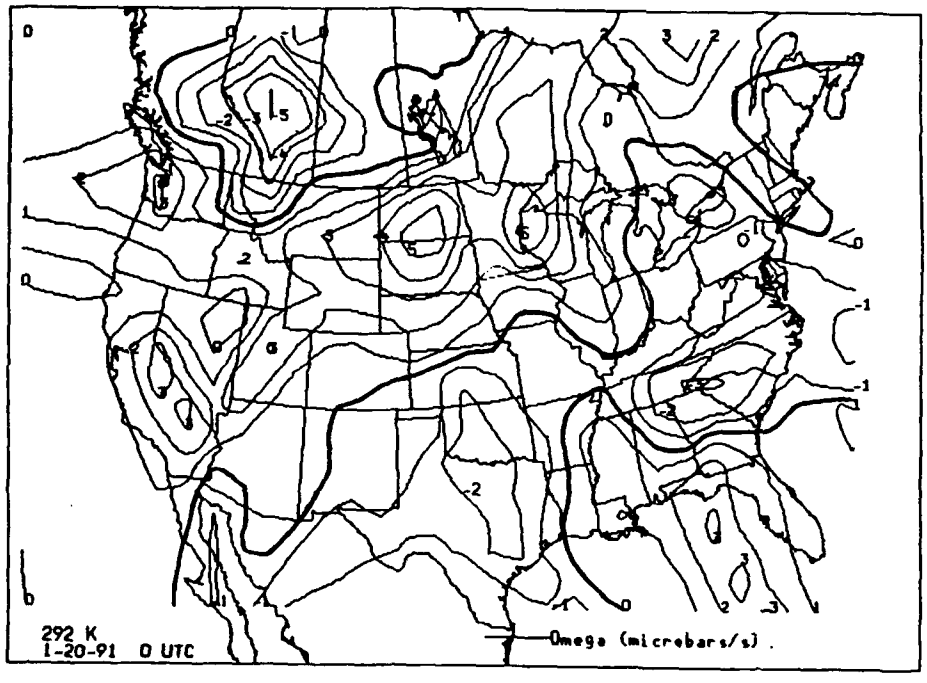

Fig. 9 Isentropic ground relative omegas on the 292 K surface in μb s^{-1} for 0000 UTC 20 January 1991.

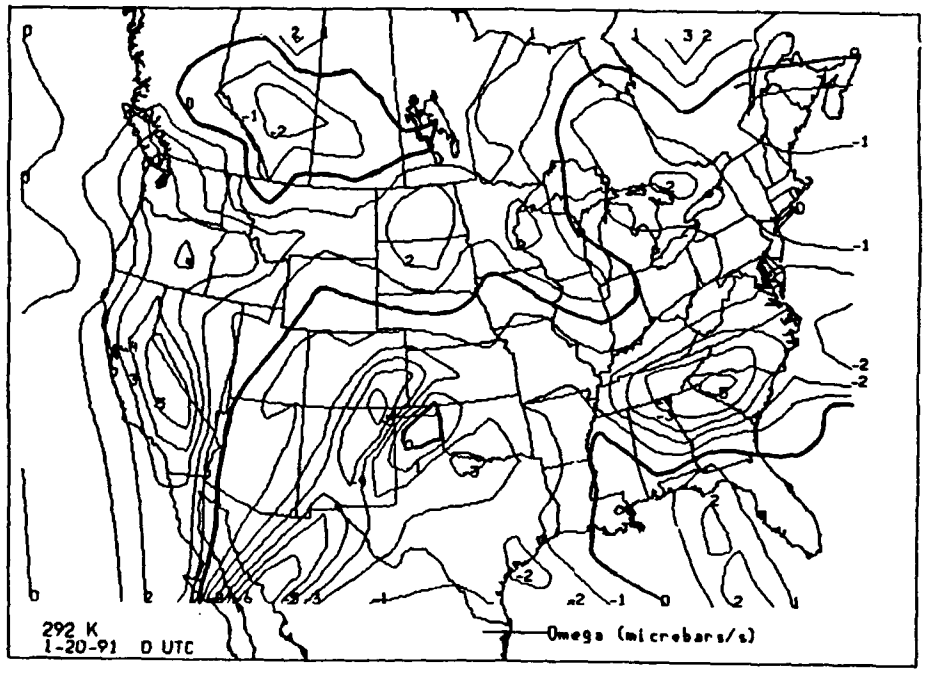

Fig. 10 Isentropic system relative omegas on the 292 K surface in μb s^{-1} for 0000 UTC 20 January 1991.

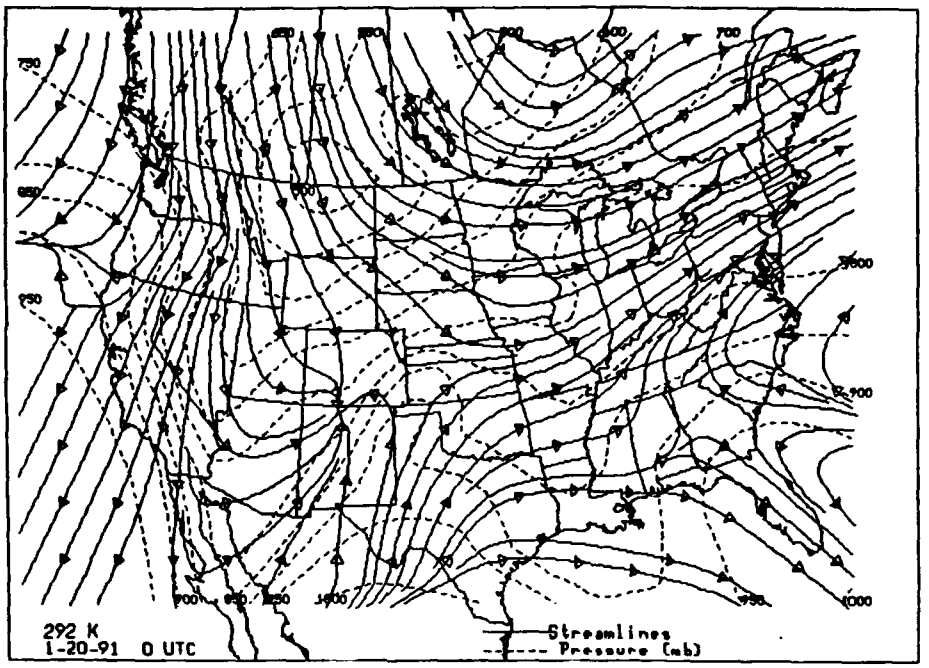

Fig. 11 Isentropic ground relative streamlines (solid lines) and pressure levels (dashed lines in mb) on the 292 K surface for 0000 UTC 20 January 1991.

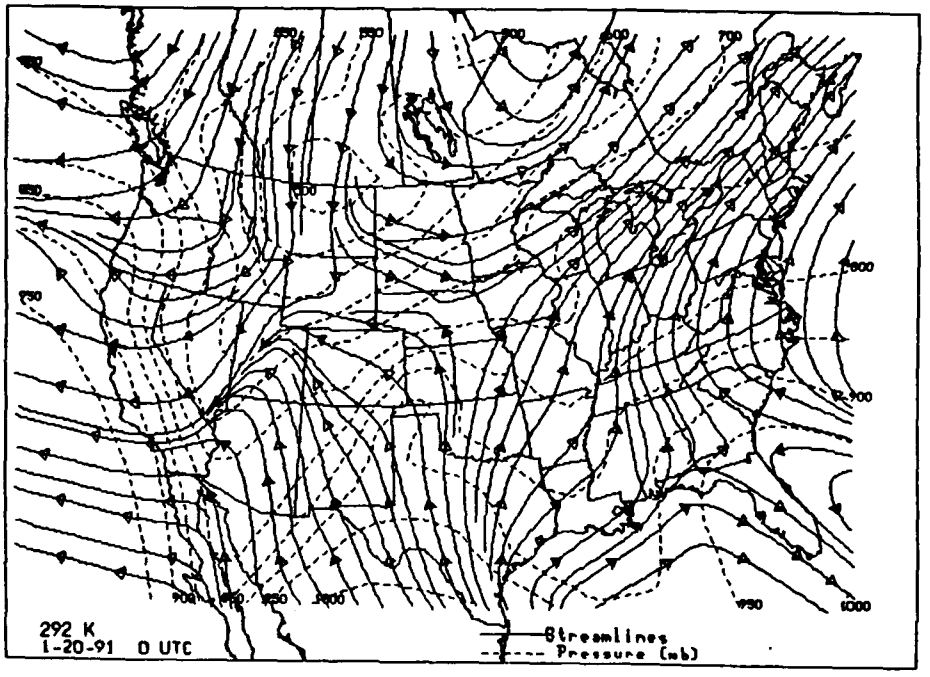

Fig. 12 Isentropic system relative streamlines (solid lines) and pressure levels (dashed lines in mb) on the 292 K surface for 0000 UTC 20 January 1991.

4.1.3 Conditional Symmetric Instability and Equivalent Potential Vorticity

As discussed above, CSI and EPV can be used to estimate regions of enhanced frozen precipitation within a larger area of light - moderate precipitation. To asses this role for this case, a vertical cross section normal to the 850-300 mb thickness lines was prepared. This cross section depicts areas of CSI along the cross section in terms of EPV as described in (9).

Figure 13 shows the 850-300 mb thickness for 0000 UTC 20 January with the cross section over Colorado. Figure 14 shows term 1 in (9). As noted earlier, this term tends to be negative. Figure 15 displays term 2 for the same time. No negative regions were generated to indicate convective instability. In a convectively stable atmosphere, term 2 can contribute to CSI by becoming nearly zero without becoming convectively unstable. Figure 16 shows the total EPV for the cross section. Two areas of EPV < 0 are indicated -- one area is near the surface, the other is a large area from 600 to 450 MB over the Denver area. Analysis of the Denver sounding (Fig. 7) reveals the average relative humidity from the surface to 850 MB is

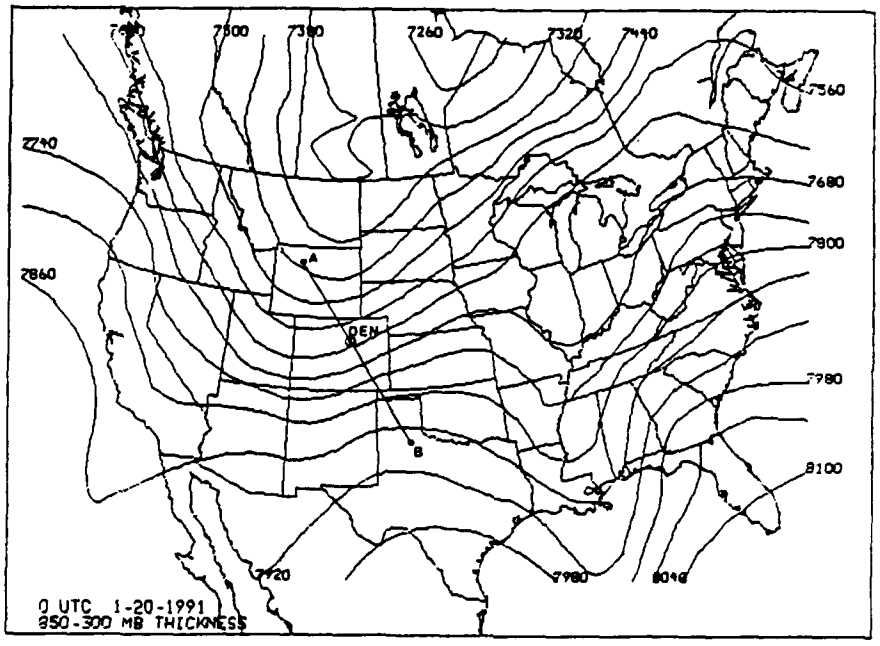

Fig. 13 850-300 mb thickness in gpm for 0000 UTC 20 January 1991. Line A-B depicts the position of cross section shown in Figs. 14-16. DEN = Denver, Colorado.

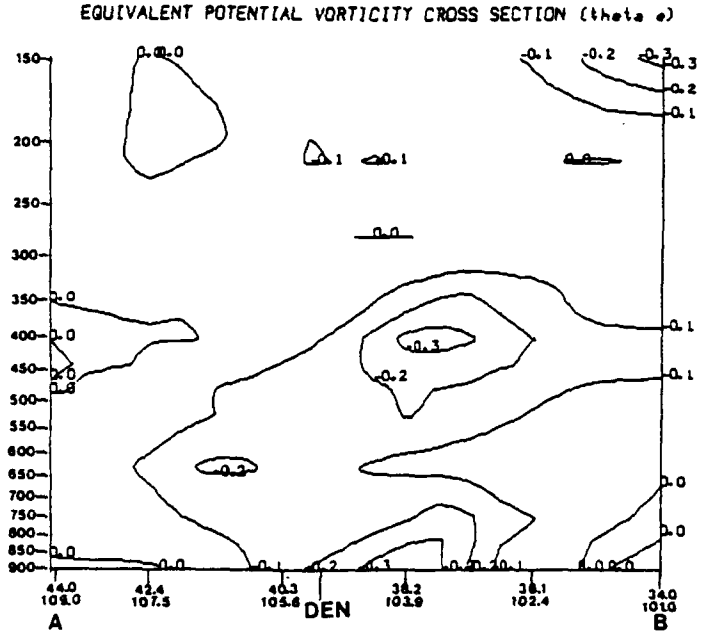

Fig. 14 Vertical cross section of term 1 of EPV in (9), in PVU (1 x 10^{-6} m^2 K s^{-1} kg^{-1}) along line A-B (see Fig. 13) for 0000 UTC 20 January 1991. DEN = Denver, Colorado.

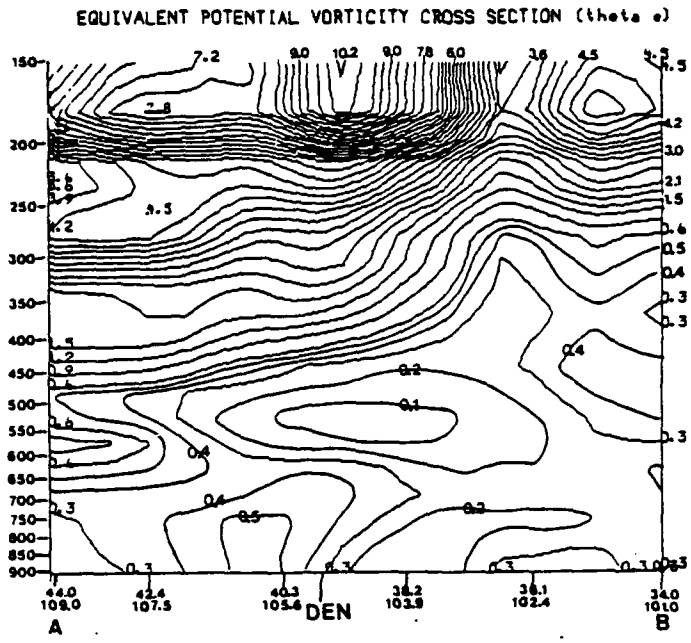

Fig. 15 Vertical cross section of term 2 of EPV (including -g factor) in (9), in PVU (1×10^{-6} m^2 K s^{-1} kg^{-1}) along line A-B (see Fig. 13) for 0000 UTC 20 January 1991. DEN = Denver, Colorado.

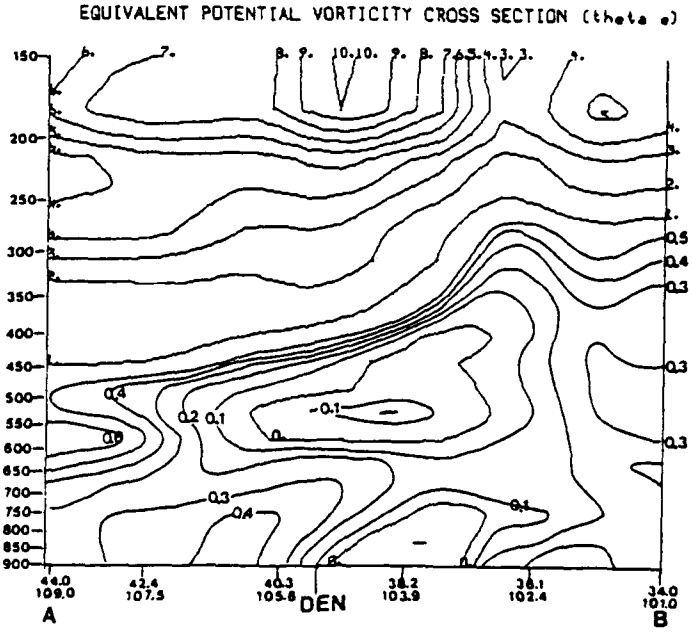

Fig. 16 Vertical cross section of EPV in PVU (1×10^{-6} m^2 K s^{-1} kg^{-1}) along line A-B (see Fig. 13) for 0000 UTC 20 January 1991. Negative region depicts CSI. DEN = Denver, Colorado.

approximately 80%, with even higher values from the surface to 700 MB. This would meet the relative humidity criterion for CSI set by Bennetts and Sharps' (1982) research. Shields et al. (1991) showed multiple precipitation bands forced by CSI, whereas a single band was caused by frontogenetical forcing. CSI in the Denver area would help explain the multiple mesoscale banded precipitation oriented parallel to the thickness within the larger synoptic scale precipitation area.

4.2 Case 2: 31 October 1991 - 2 November 1991

4.2.1 Synoptic Overview

A long wave trough developed in the upper air over the southwestern United States on 30 October 1991. By 0000 UTC 1 November (Fig. 17) major, rapid development occurred over the panhandle of Oklahoma. Over the next 36 hours the upper level low became negatively tilted as it moved to the north-northeast.

At 0000 UTC 31 October a weak surface low developed along a cold front in southern Texas. This low moved rapidly to the north-northeast and by 1200 UTC 1 November was centered over southeast Iowa with a

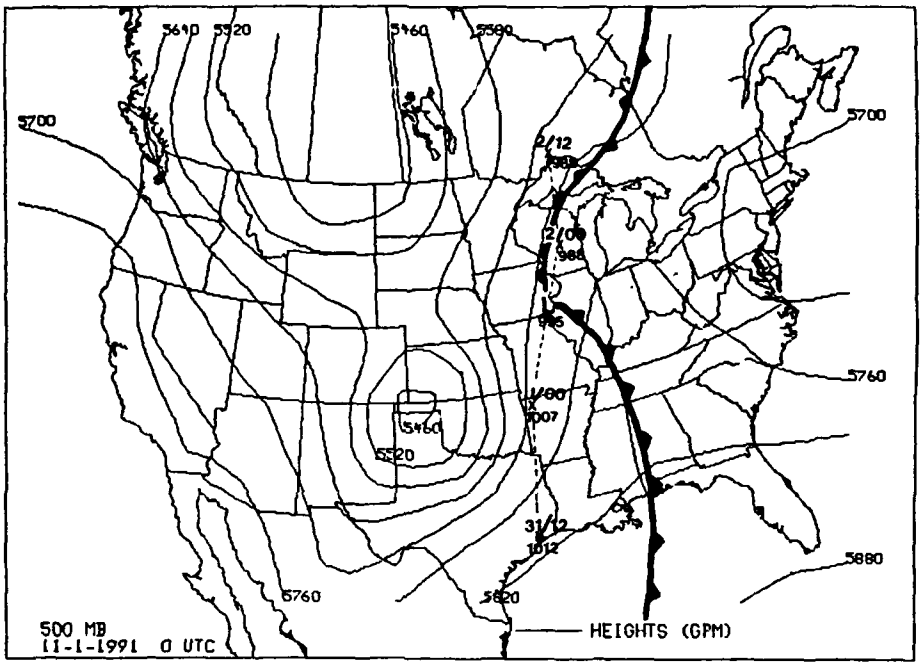

Fig. 17 500 mb chart for 0000 UTC 1 November 1991. Height in geopotential meters (gpm). Surface features for 1200 UTC 1 November 1991. X's mark position of surface low and pressure in time from 1200 UTC 31 October 1991 to 1200 UTC 2 November 1991.

central pressure of 996 mb (Fig. 17). A cold front extended south from the low pressure center through Illinois, Kentucky, Tennessee, and eastern Alabama into the Gulf of Mexico. A warm front stretched north from the low's center through extreme eastern Iowa into Wisconsin. During the next 24 hours the storm moved from southeastern Iowa through Wisconsin into southern Ontario and the surface low deepened another 7 mb to 988 mb.

This storm produced heavy snow, ice, freezing rain, and ice pellets across the upper Midwest. The intense low pressure moving along the frontal boundary caused blizzard conditions across Iowa, Minnesota, and Wisconsin. Snowfall rates occasionally ranged from 2.5 to 5 cm (1 to 2 in) an hour over eastern Minnesota. A number of long-standing snowfall records fell at the Duluth and Twin Cities National Weather Services' offices (see Fig. 18). The Twin Cities office dubbed this storm "The Great Holloween Snowstorm".

4.2.2 Isentropic Vertical Motion and Streamlines

To gain the best insight into the atmospheric motion of this storm, the 300 K isentropic surface was

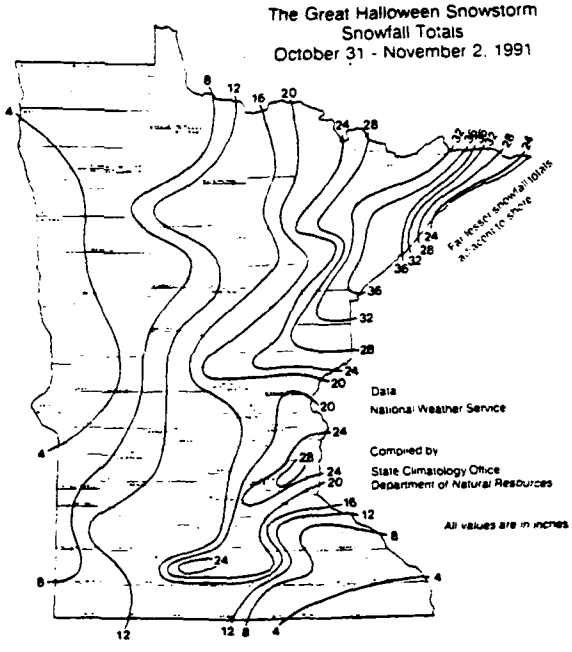

Fig. 18 Snowfall totals (inches) over the state of Minnesota from 31 October to 2 November 1991. (Storm Data 1991c).

used. The S-R vertical motion values (Fig. 19) are stronger and the centers more accurately placed than the G-R vertical motion (not shown). Infrared MB enhancement curve imagery (Fig. 20) and winter enhancement curve imagery (Fig. 21) cloud patterns for 0000 UTC 1 November are well-correlated with the S-R omega centers. Beckman (1987) found that clouds in satellite imagery seldom match instantaneous vertical motion. This is because clouds seen on satellite imagery are the net result of vertical motions which air parcels have experienced for several hours.

The S-R streamlines for 0000 UTC 1 November (Fig. 22) reveal a southeasterly flow with air rising to approximately 750 mb over the maximum snow area. The lifted condensation pressure data (not shown) revealed the air needed to rise to the 750 mb level to reach saturation over the same area.

4.2.3 Frontogenetical Forcing

To assess the role of frontogenetical forcing, the form of the frontogenetical function in (10) was used to compute frontogenesis for the upper air. Figures 23 and 24 show the 1000-500 mb thickness pattern for 0000

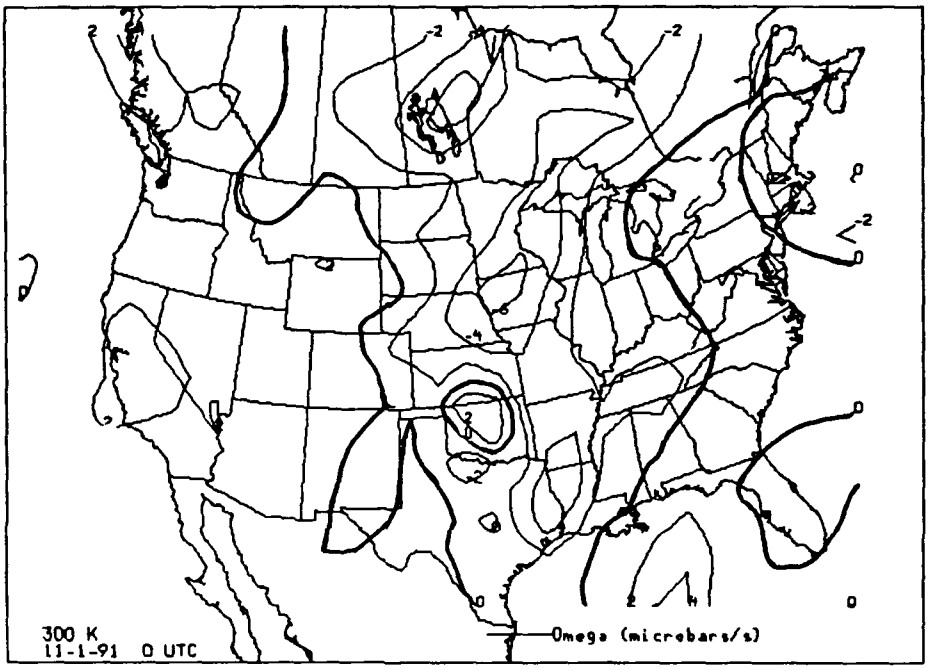

Fig. 19 Same as Fig. 10, except for 0000 UTC 1 November 1991.

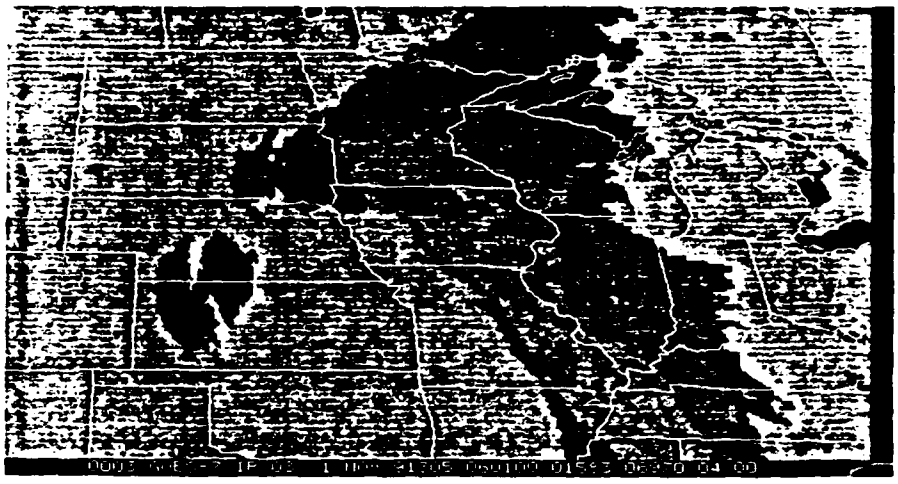

Fig. 20 Satellite imagery using the MB enhancement curve for 0600 UTC 1 November 1991.

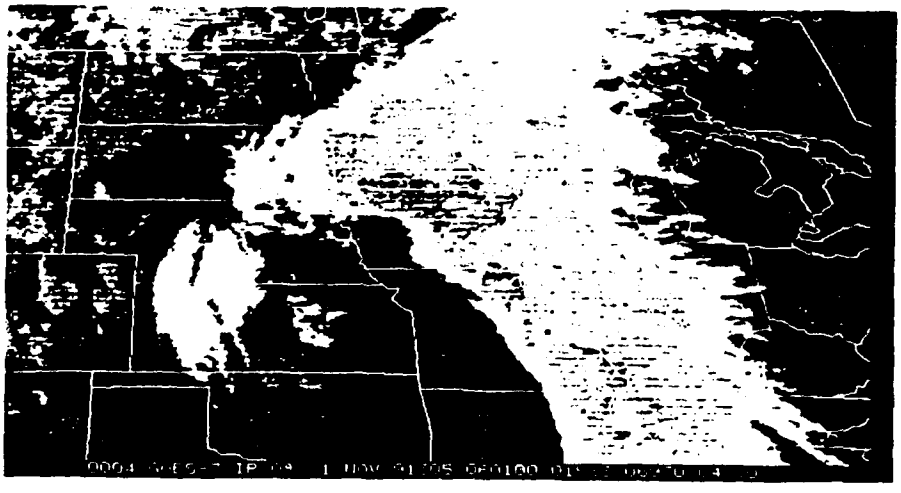

Fig. 21 Satellite imagery using a winter enhancement curve for 0600 UTC 1 November 1991.

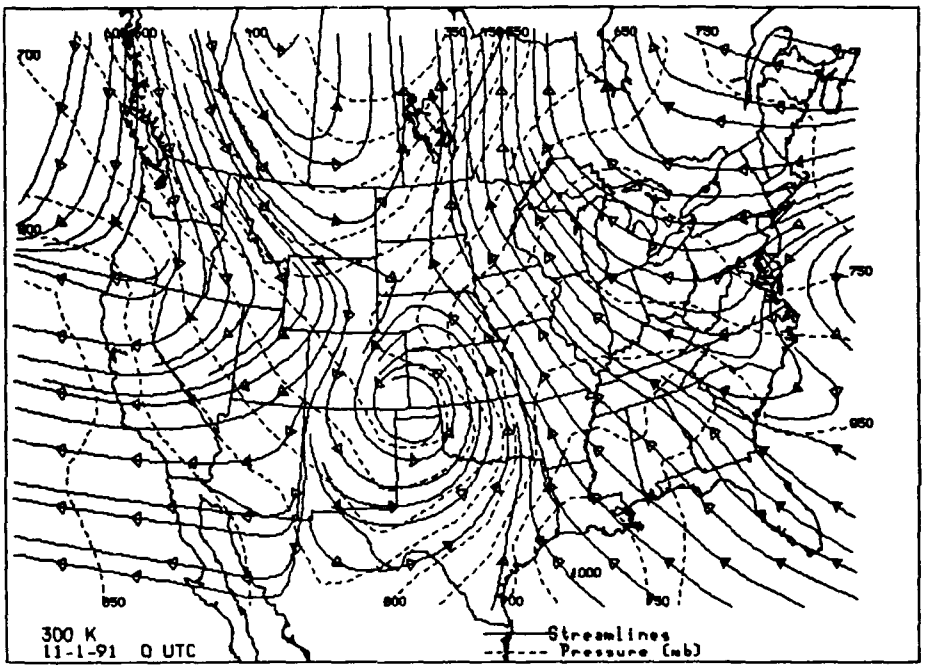

Fig. 22 Same as Fig. 12, except for 0000 UTC 1 November 1991.

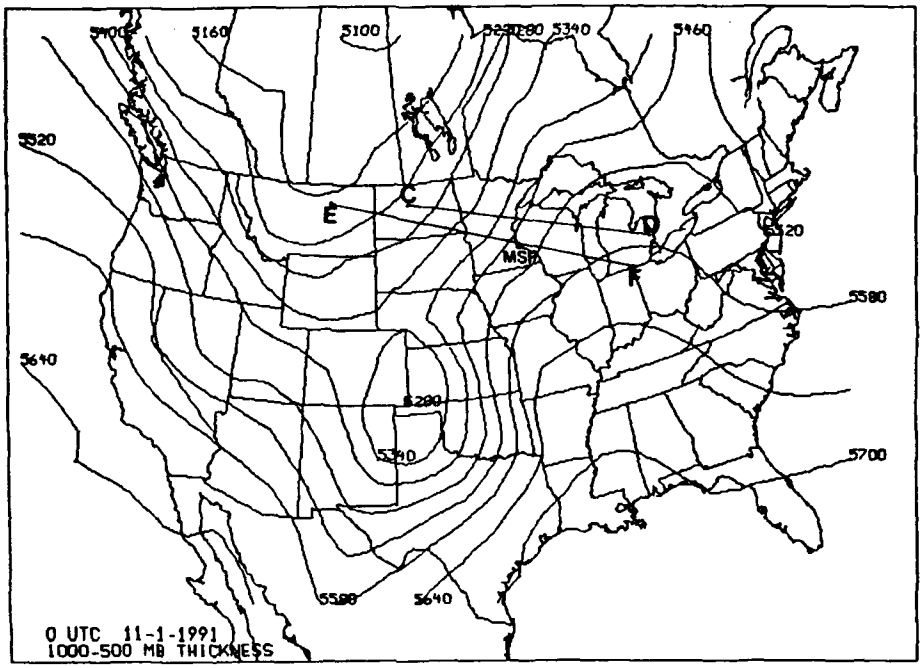

Fig. 23 Same as Fig. 13, except for 0000 UTC 1 November 1991. MSP = Minneapolis, Minnesota.

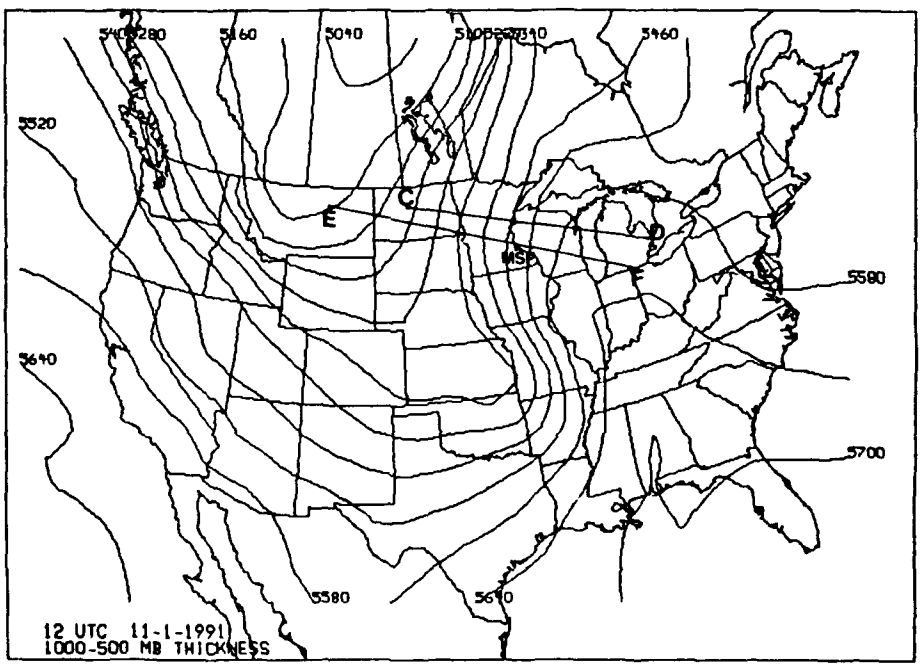

Fig. 24 Same as Fig. 13, except for 1200 UTC 1 November 1991. MSP = Minneapolis, Minnesota.

UTC 1 November and 1200 UTC 1 November, respectively, and the location of the cross sections labeled C-D and E-F, used for this case.

At 700 mb for 0000 UTC 1 November an area of maximum frontogenesis lies to the northwest of the surface low pressure center and frontal zones with a maxima of 15 x 10^{-10} K m^{-1} s^{-1} in northwest Iowa (Fig. 25). A vertical cross section of the two-dimensional frontogenetical function taken along both lines C-D and E-F in Fig. 23 reveals the structure of this frontogenetical zone (Figs. 26-27). The two cross sections depict the greatest frontogenesis as taking place at approximately 650 - 700 mb with a secondary maxima in middle levels. The frontogenetical zone sloped to the east in both cross sections.

As described earlier, kinematic omegas were computed for this case to diagnose the direct thermal circulation (DTC) branches of UVM and DVM created by the forcing of frontogenesis. Figures 28 and 29 show the moderate-strong ascent was part of a thermally direct ageostrophic circulation created by frontogenetical forcing. In these diagrams the horizontal component of the arrow represents the component of the ageostrophic wind in the plane of the

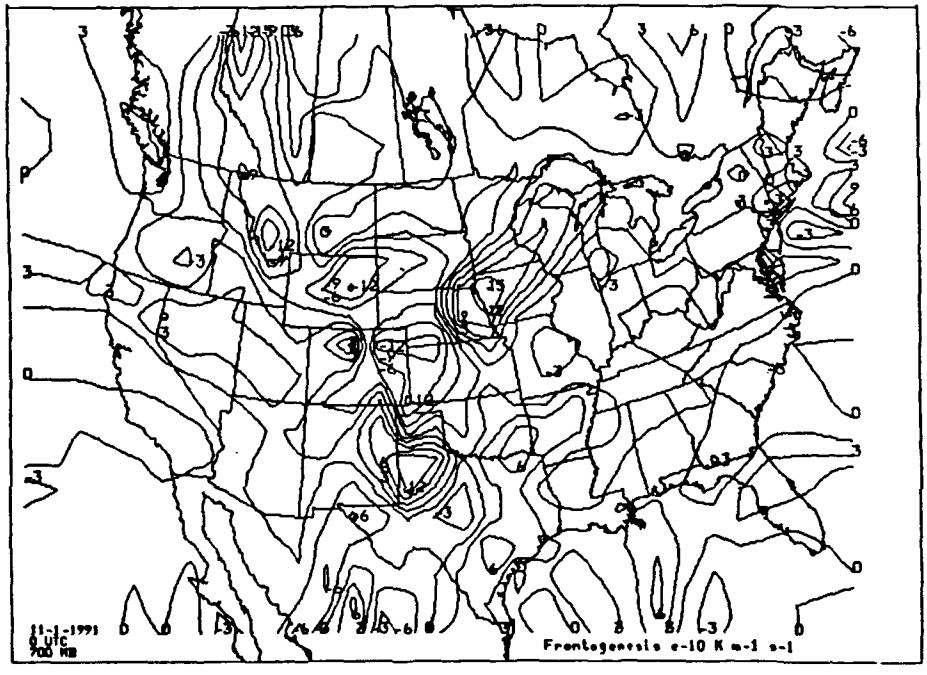

Fig. 25 Frontogenetical forcing (x 10^{-10} K m^{-1} s^{-1}) at 700 mb for 0000 UTC 1 November 1991.

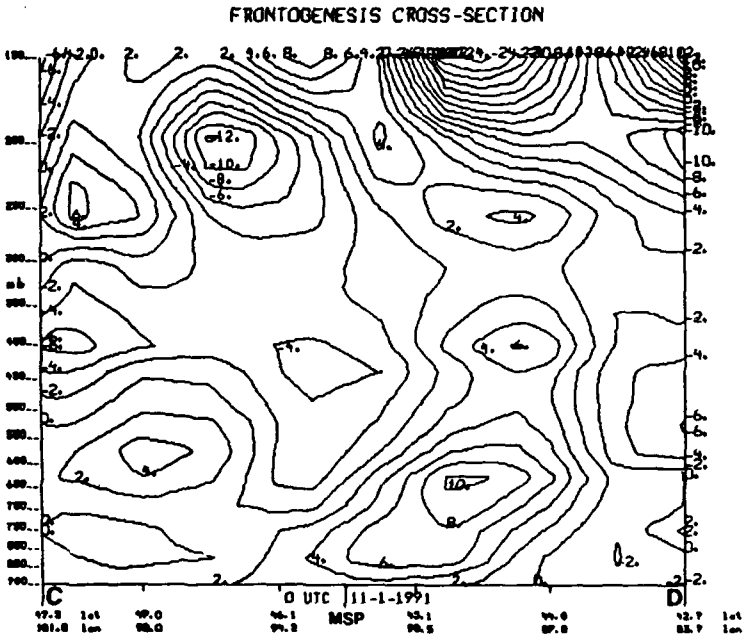

Fig. 26 Cross section of two-dimensional frontogenesis (x 10^{-10} K m^{-1} s^{-1}) taken along line C-D in Fig. 23 for 0000 UTC 1 November 1991. MSP = Minneapolis, Minnesota.

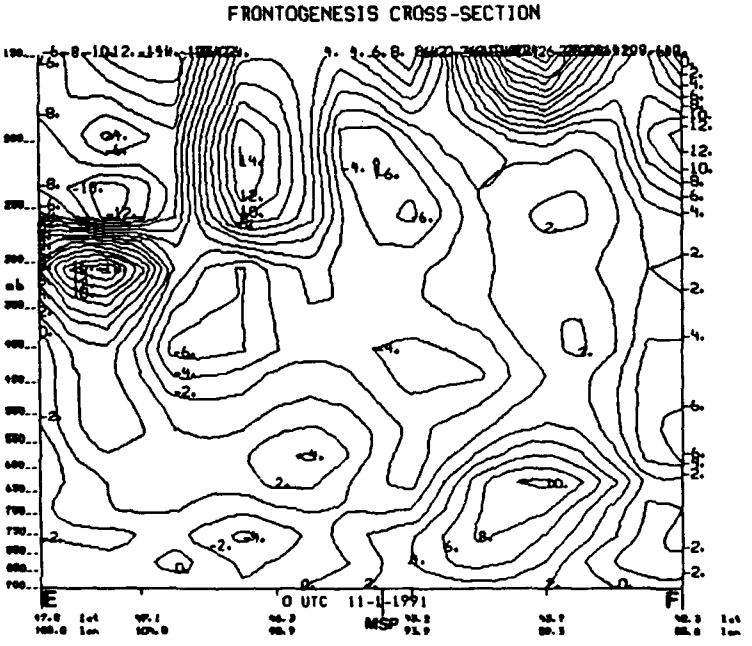

Fig. 27 Same as Fig. 26, except along line E-F in Fig. 23. MSP = Minneapolis, Minnesota.

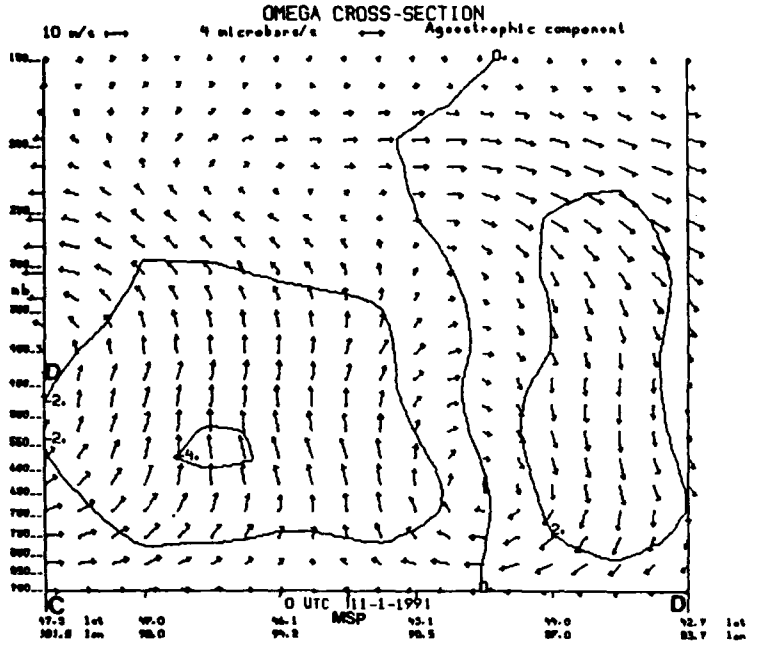

Fig. 28 Vertical cross section of ageostrophic winds in the plane of the cross-section (horizontal component of arrows, m s^{-1}) and kinematic omegas (vertical component of arrows, μb s^{-1}) along the line C-D shown in Fig. 23 for 0000 UTC 1 November 1991. Solid lines are vertical motion in μb s^{-1}.
D = DTC. I= Indirect thermal circulation.
MSP = Minneapolis, Minnesota.

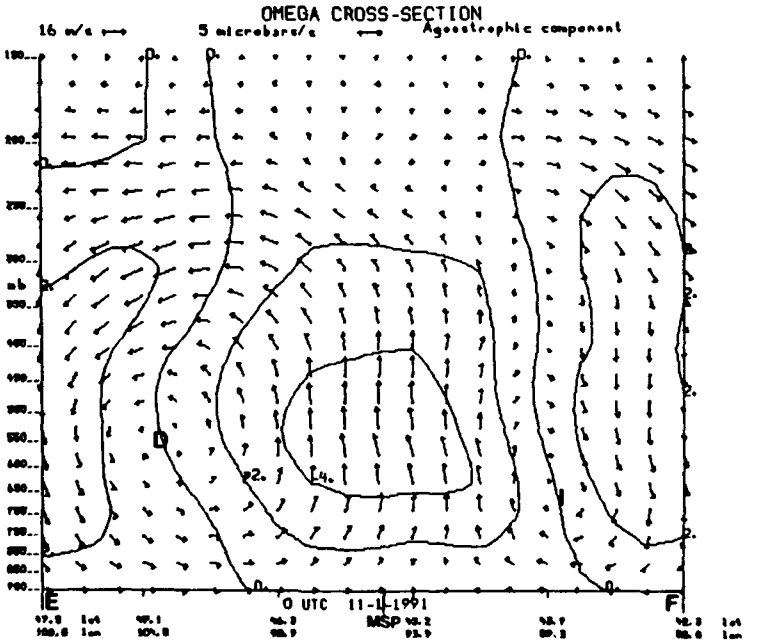

Fig. 29 Same as Fig. 28, except along line E-F in Fig. 23. D = DTC. I = Indirect thermal circulation. MSP = Minneapolis, Minnesota.

cross section taken along the line shown in Fig. 23. The vertical component of the arrow represents the vertical motion. As is graphically shown in these two cross sections, a DTC forms over an area centered on Minneapolis, Minnesota (MSP). Figures 30 and 31 show continued strong ascent for 1200 UTC 1 November along the cross section shown in Fig. 24. The DTC remains over the area centered on Minneapolis, Minnesota. Reports of the heaviest precipitation rates occurred over this area during these times of enhanced UVM by frontogenetical forcing.

4.2.4 Upper-Level Jet Secondary Ageostrophic Circulations

In this case, there is also evidence of coupled jet streak circulations enhancing the vertical motion, precipitation rates, and development rates of MPSs within the ETC. This case reinforces the evidence because the transverse circulations associated with separate jet streaks merged to focus a region of ascent that, in turn, contributed to the rapid development of the snow area. While it is true that frontogenetical forcing had a major role in the storm's development, the coupling of the jet streak circulations and the

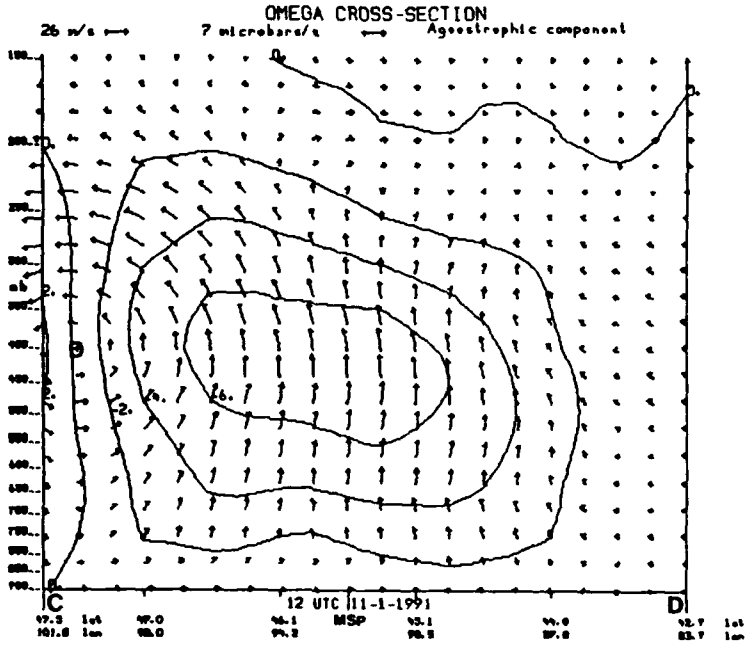

Fig. 30 Same as Fig. 28, except along line C-D in Fig. 23 for 1200 UTC 1 November 1991. D = DTC. MSP = Minneapolis, Minnesota.

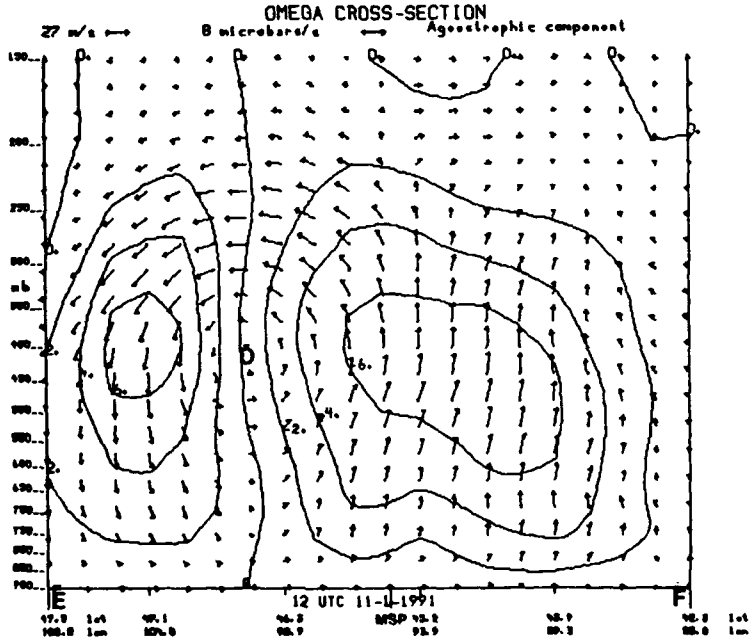

Fig. 31 Same as Fig. 28, except along line E-F in Fig. 23 for 1200 UTC 1 November 1991. D = DTC. MSP = Minneapolis, Minnesota.

related enhancement of the low-level thermal circulation pattern indicate the jet streak circulation also strengthened the vertical motion field.

The upper-level flow regime for this case was marked by the presence of two separate, nearly straight-line jet streaks, located near the 300 mb level (Fig. 32). One jet, with maximum wind speeds in its core exceeding 60 m s^{-1}, ran from central Nebraska northward into western Ontario. The other jet streak, with a region of maximum winds approaching 50 m s^{-1}, lay through western Texas. The exit region of the southern jet streak was located over western Kansas, within 300 km of the well-defined entrance region of the northern jet.

By 0000 UTC 1 November (Fig. 33) the northern jet had propagated slightly north and west. The southern jet had strengthened by 5 m s^{-1} over central Texas with its exit region pushing into eastern Kansas. The ascending branch of the thermally direct circulation in the entrance region of the northern jet streak becomes collocated with the ascending branch of the thermally indirect circulation of the southern jet streak. By 1200 UTC 1 November (Fig. 34) the northern jet's core had migrated west into North Dakota and southern

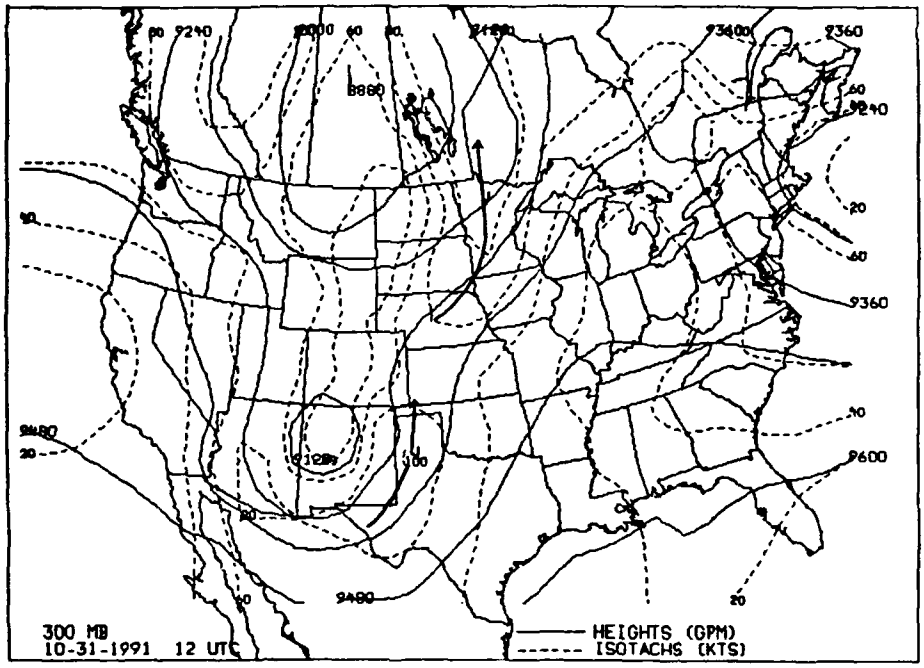

Fig. 32 300 mb chart for 1200 UTC 31 October 1991. Height (solid lines) in gpm and isotachs (dashed lines) are in knots (kts). Heavy solid lines indicate jet cores.

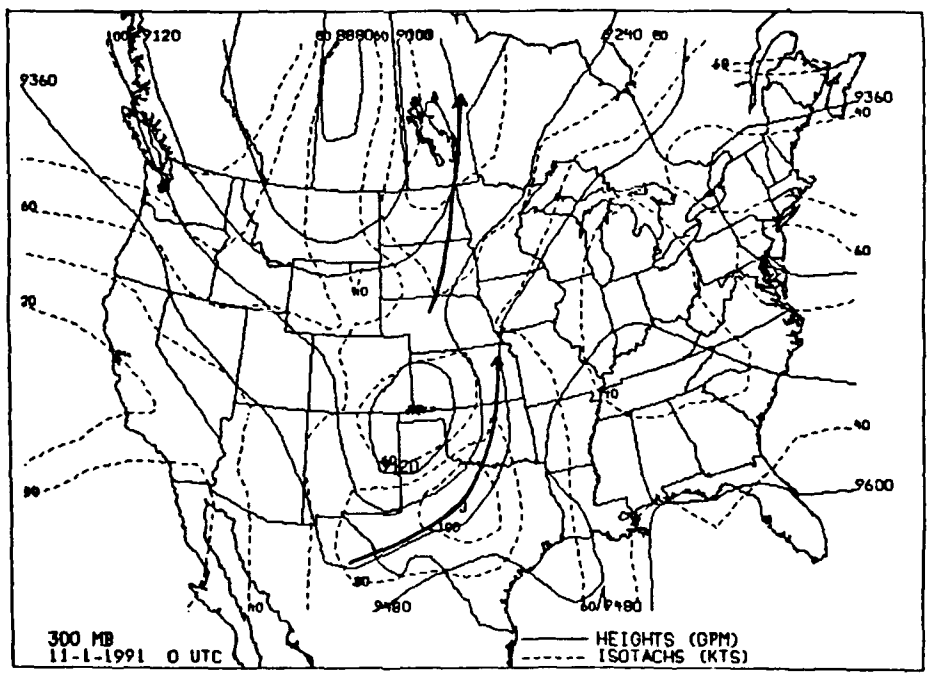

Fig. 33 Same as Fig. 32, except for 0000 UTC 1 November 1991.

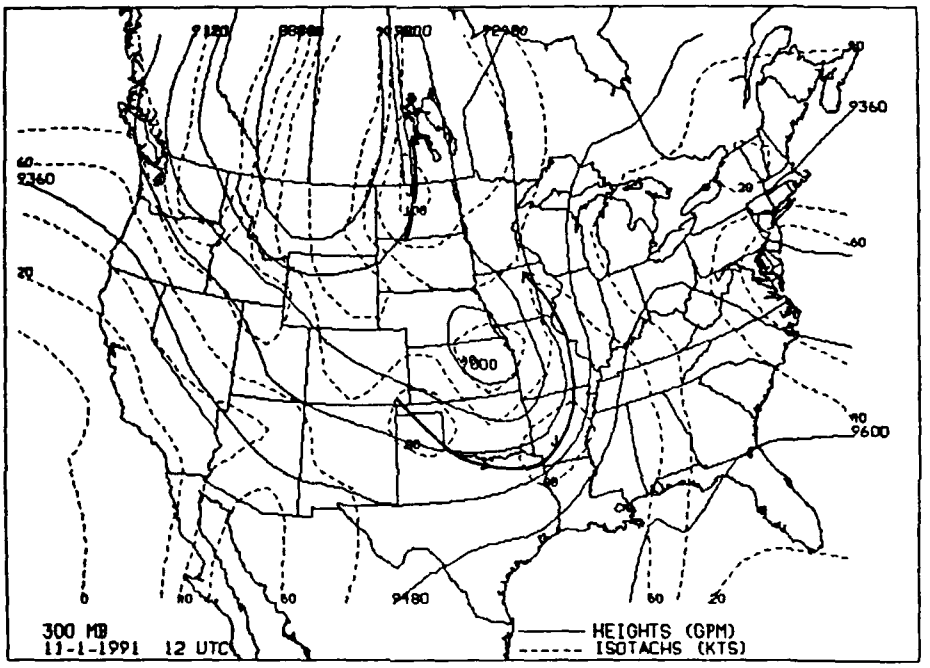

Fig. 34 Same as Fig. 32, except for 1200 UTC 1 November 1991.

Manitoba, but it had broadened with 30 - 40 m s^{-1} winds over Minnesota. The southern jet curves from northwest Texas into central Arkansas and eastern Missouri with its exit region over northwest Iowa. The two jets continue to be collocated, likely contributing to the heavy snowfall of this storm. The DTC of the northern jet appears to be enhanced as the exit region of the southern jet moves north.

4.3 Case 3: 27-28 December 1990

4.3.1 Synoptic Overview

An upper-level shortwave trough and vorticity maximum developed over Colorado and eastern Kansas at 1200 UTC 27 December 1990 (Fig. 35). This trough moved through the mid-Mississippi River Valley into the Great Lakes region over the next 24 hours.

At 1200 UTC 27 December a weak surface low had developed off the coast of Texas in the Gulf of Mexico (Fig. 36). An inverted trough (axis of low pressure directed to the north) extended north into eastern Texas. Comparison of the 1200 UTC 27 December surface map to the 1200 UTC 28 December surface map (not shown) reveals that the inverted trough developed

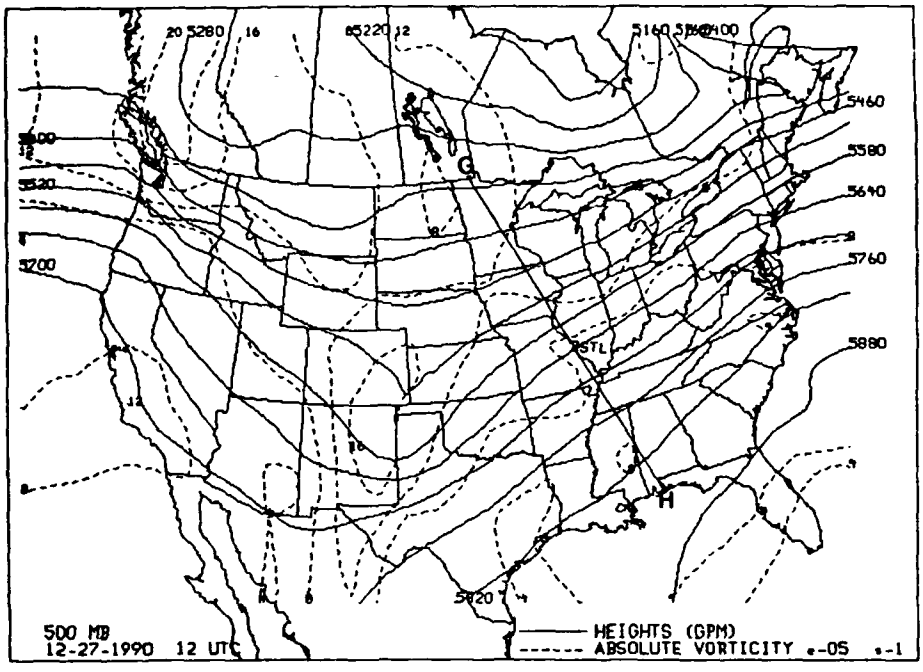

Fig. 35 Same as Fig. 6, except for 1200 UTC 27 December 1990. STL = St. Louis, Missouri.

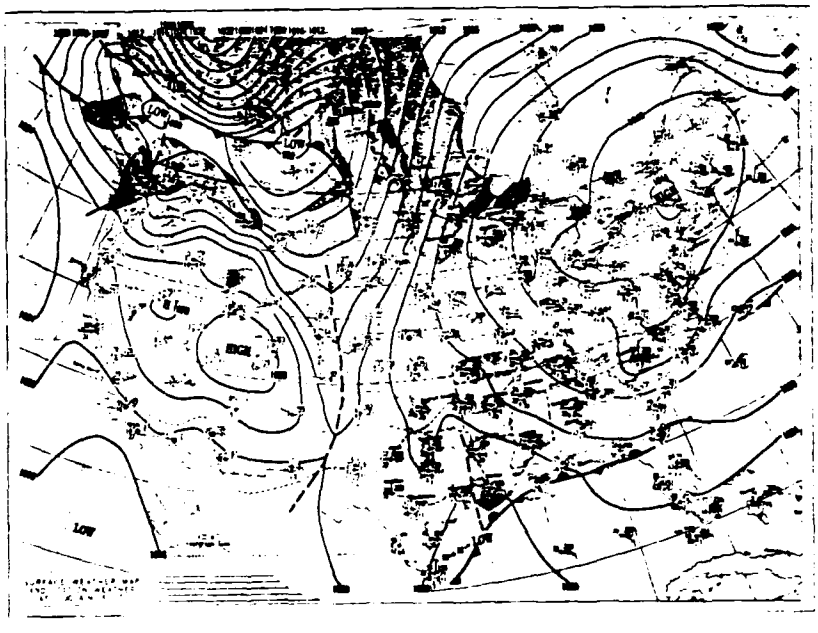

Fig. 36 Surface weather map at 1200 UTC 27 December 1990. (Daily Weather Maps 1990)

northeastward into western Tennessee, Kentucky, southern Illinois, southern Indiana, and Ohio.

A band of heavy snow formed to the north and west of this inverted trough as it developed during 27 December. Snow accumulated 15 to 25 cm (6 to 10 in) 50 km south of St. Louis, Missouri, with 8 to 15 cm (3 to 6 in) accumulation reported in the city of St. Louis and surrounding area. The snow band stretched from central Missouri, into Ohio and the southwestern corner of Wisconsin (Fig. 37).

4.3.2 Isentropic Vertical Motion and Streamlines

The 292 K isentropic surface was used for this case because it intersected the region of baroclinicity and moisture. The S-R vertical motion values for 1200 UTC 27 December (Fig. 38) are much stronger than the G-R values (not shown). The G-R values for St. Louis and vicinity are approximately -2 $\mu b\ s^{-1}$ while the S-R values range from -4 to -8 $\mu b\ s^{-1}$ from St. Louis into the Gulf States. On the south side of the upper-level trough, the S-R vertical motions also reveal a larger area of UVM than the G-R vertical motion values. This

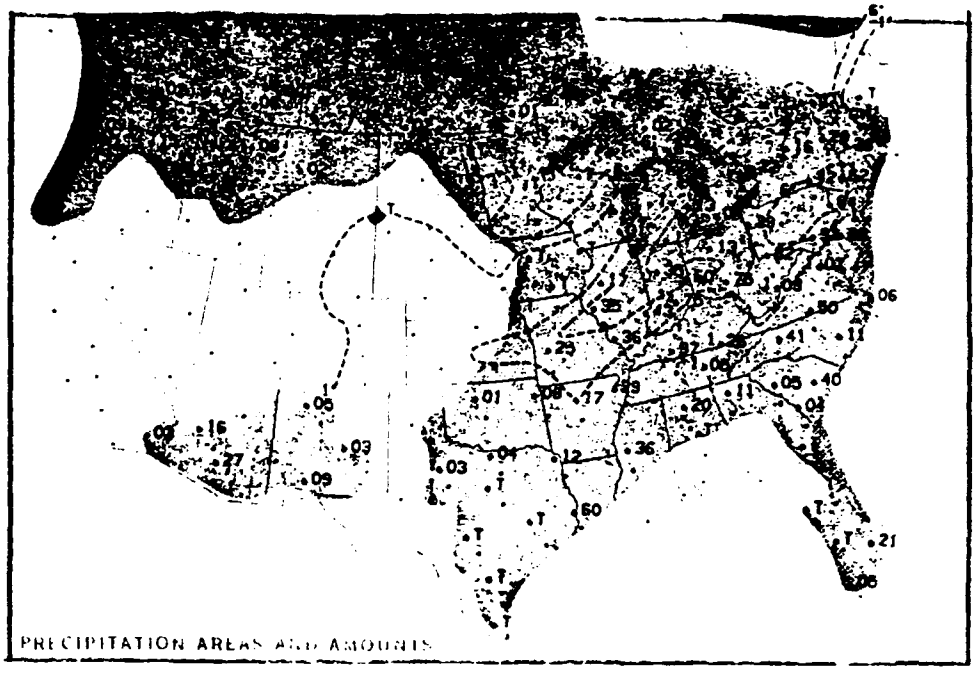

Fig. 37 24 hour precipitation and amounts for 1200 UTC 27 December to 1200 UTC 28 December 1990. (Daily Weather Maps 1990)

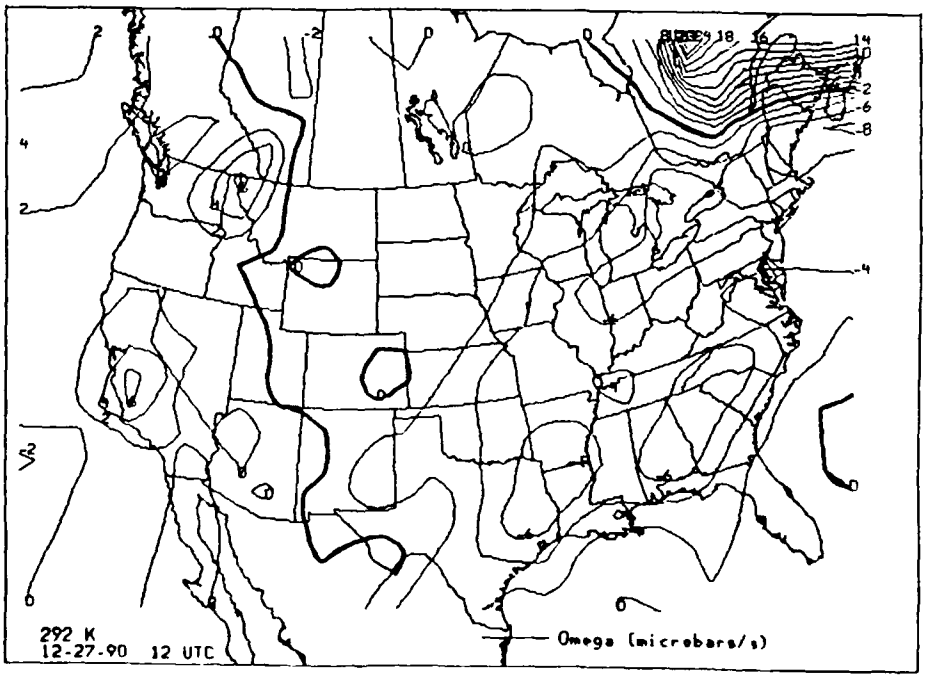

Fig. 38 Same as Fig. 10, except for 1200 UTC 27 December 1990.

stronger, larger area provided the forcing necessary to lift the air to saturation.

The S-R streamlines are also more representative of atmospheric motions for this storm. G-R streamlines (not shown) show the inflow into the storm from the south-southwest, almost parallel to the pressure surfaces, rising to approximately the 750 mb level. However, the S-R streamlines for 1200 UTC 27 December (Fig. 39) indicate southeasterly inflow with air rising to approximately the 750 mb level. Note the streamlines crossing the pressure level contours at nearly a 90^{o} angle -- indicating greater lifting.

4.3.3 Upper-Level Jet Secondary Ageostrophic Circulations

The 300 mb height and isotach charts for 1200 UTC 27 December (Fig. 40) show a southwesterly jet streak through the central United States with a jet core > 70 m s^{-1} (140 kts) over Lake Erie. By 0000 UTC 28 December (Fig. 41), the jet axis becomes more westerly near the jet streak entrance region over New Mexico and northern Texas while the 70 m s^{-1} wind maximum moves off into southeastern Canada.

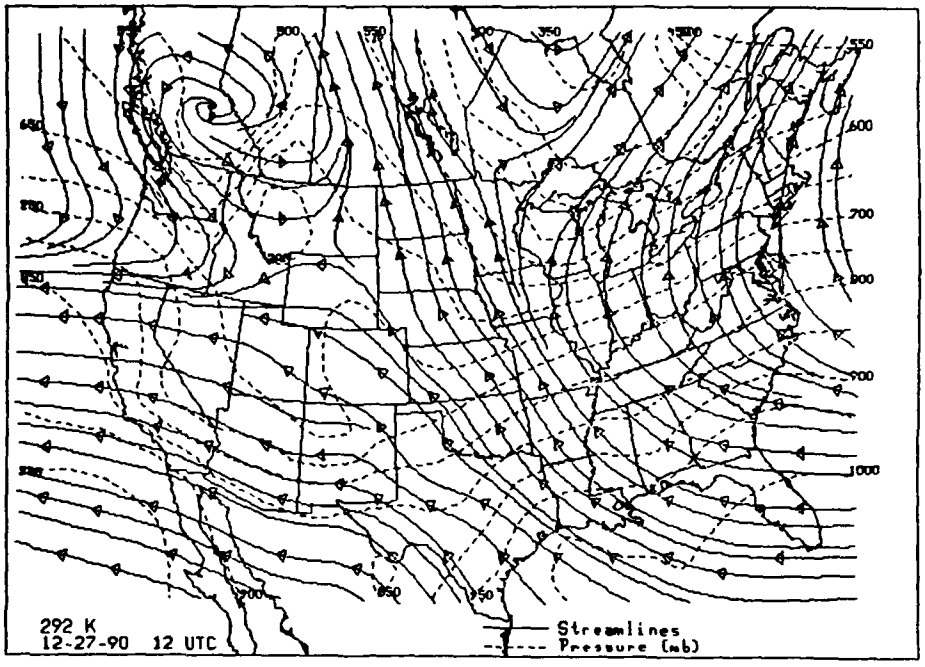

Fig. 39 Same as Fig. 12, except for 1200 UTC 27 December 1990.

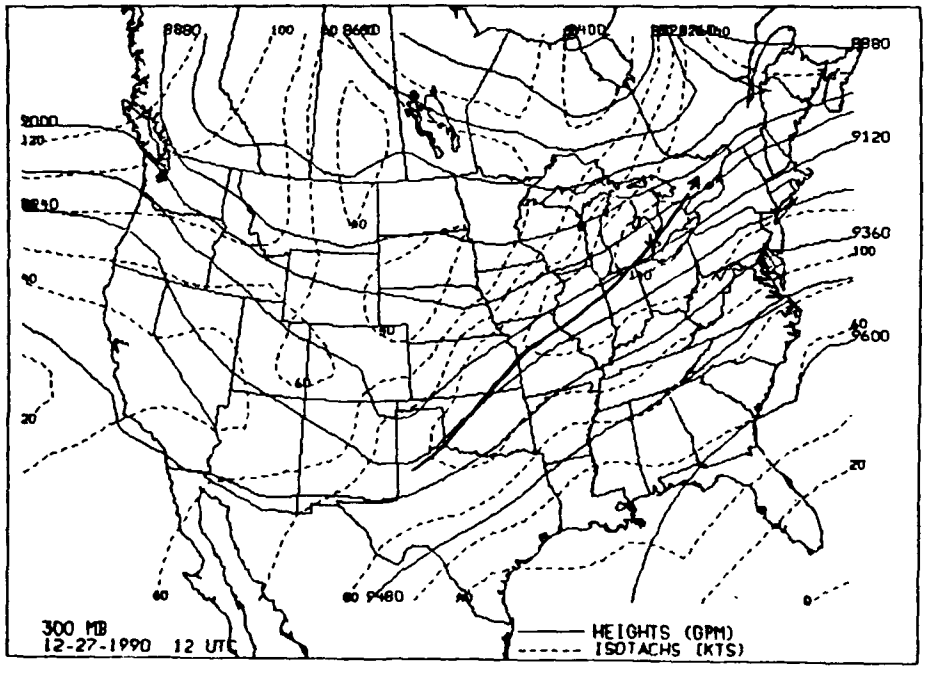

Fig. 40 Same as Fig. 32, except for 1200 UTC 27 December 1990

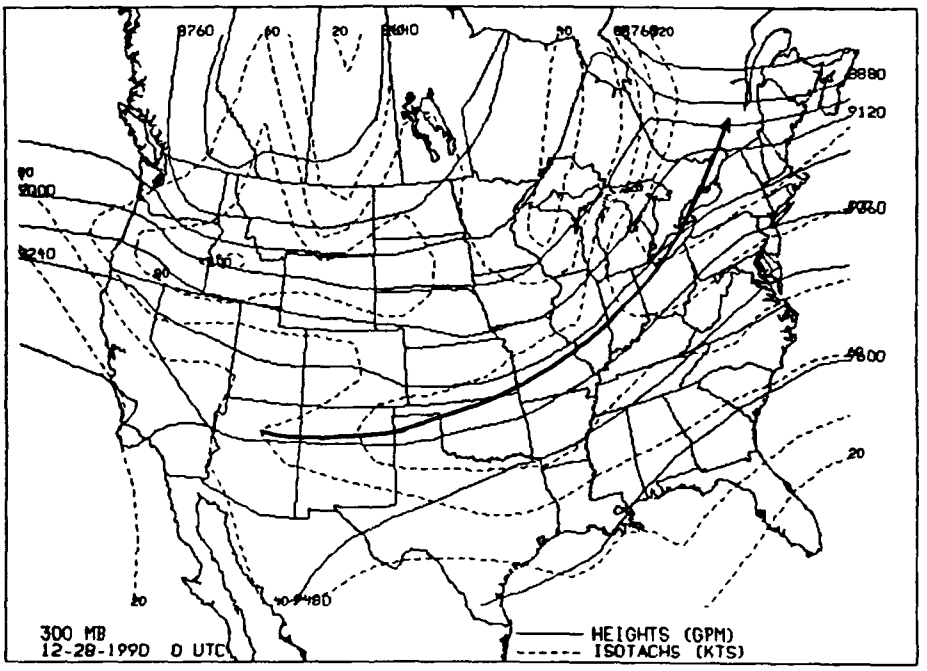

Fig. 41 Same as Fig. 32, except for 0000 UTC 28 December 1990.

A cross section of the tangential ageostrophic component of the wind and vertical motion (Fig. 42) for 1200 UTC 27 December along line G-H in Fig. 35 shows a DTC in the entrance region of the jet streak. The strongest value of UVM is -6 $\mu b\ s^{-1}$. Comparing Fig. 42 with Fig. 35 reveals that the mesoscale area of UVM correlates very well with the synoptic-scale area of S-R vertical motion values, and both have approximately the same strength.

4.3.4 Conditional Symmetric Instability and Equivalent Potential Vorticity

EPV was computed along the line G-H (Fig. 35) to diagnose CSI near the area of snow. Figure 43 shows the total EPV along the cross section G-H. Two areas of negative EPV are evident, one south of St. Louis (STL) from 750 mb to approximately 550 mb and a larger area aloft. Comparing Fig. 43 with the cross section of the tangential ageostrophic component of the wind and vertical motion in Fig. 42 reveals that the CSI is strongest in the region of the DTC. The greatest snowfall occurred approximately 50 km to the south of STL at this time, in the same region where CSI and the entrance region jet DTC co-exist. CSI apparently

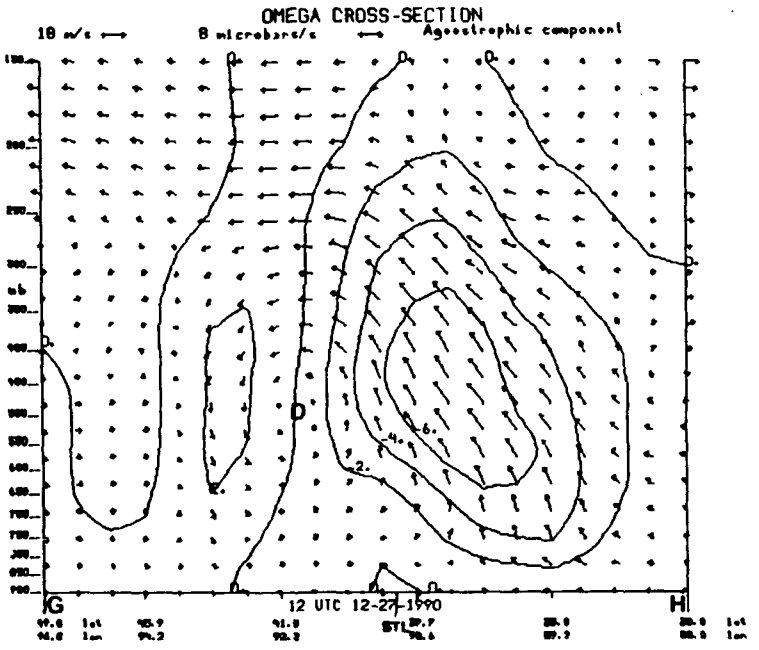

Fig. 42 Same as Fig. 28, except along line G-H in Fig. 35 for 1200 UTC 27 December 1990. D = DTC. STL = St. Louis, Missouri.

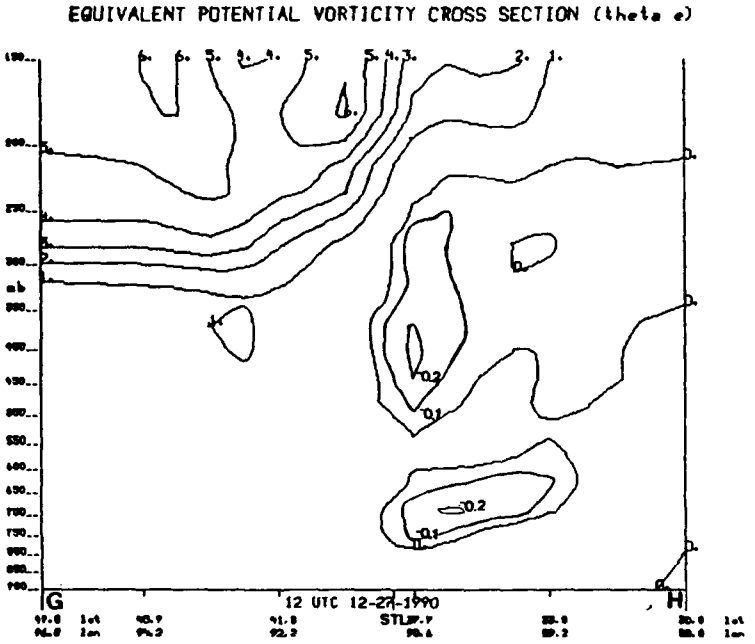

Fig. 43 Same as Fig. 16, except along line G-H in Fig. 35 for 1200 UTC 27 December 1990. STL = St. Louis, Missouri.

helped to initiate slantwise convection in the region and the DTC enhanced and focused the UVM. The two forcing mechanisms likely combined to produce the mesoscale band of heavy snowfall.

4.4 Case 4: 20-22 April 1992

4.4.1 Synoptic Overview

A long wave trough developed at 500 mb over the central United States on 20 April 1992. This trough intensified into a closed low over northwest Iowa by 0000 UTC 21 April (not shown).

At the surface a low developed along a cold front in northwest Arkansas. By 0000 UTC 21 April the low had intensified to 996 mb and moved into northwest Iowa (Fig. 44), stacking vertically under the upper-level low. A cold front extended from the low through eastern Iowa, western Kansas, Oklahoma, and Colorado.

A band of moderate snow formed to the west of the low and the cold front (Fig. 45). The snow band extended from northeast Kansas to northeast South

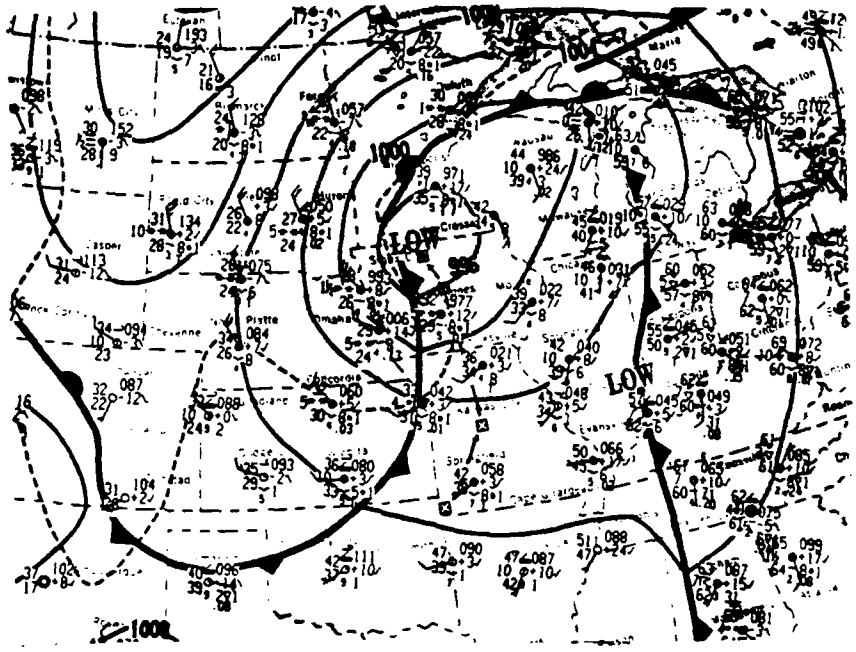

Fig. 44 Same as Fig. 36, except for 1200 UTC 21 April 1992.
(Daily Weather Maps 1992)

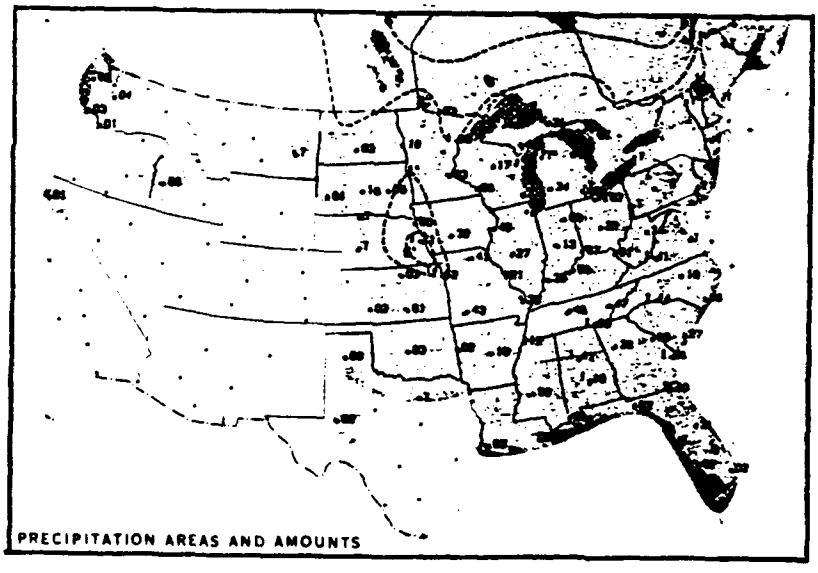

Fig. 45 Same as Fig. 37, except for 1200 UTC 20 April to 1200 UTC 21 April 1992.
(Daily Weather Maps 1992)

Dakota. Snow accumulated to over 15 cm (6 in) in the Omaha, Nebraska area on 20-21 April.

4.4.2 Isentropic Vertical Motion and Streamlines

The 300 K isentropic surface was used for this case. The S-R vertical motion values for 0000 UTC 21 April (Fig. 46) are stronger and the centers more accurately placed than the G-R values (not shown). Infrared MB enhancement curve imagery (Fig. 47) and winter enhancement curve imagery (Fig. 48) cloud patterns for 0100 UTC 21 April are well-correlated with the S-R omega centers.

The S-R streamlines for 0000 UTC 21 April (Fig. 49) reveal an east-northeasterly flow with air rising to approximately 700 mb over the maximum snow area. The lifted condensation pressure data (not shown) showed the air needed to rise to between the 700 and 650 mb levels to reach saturation over the same area.

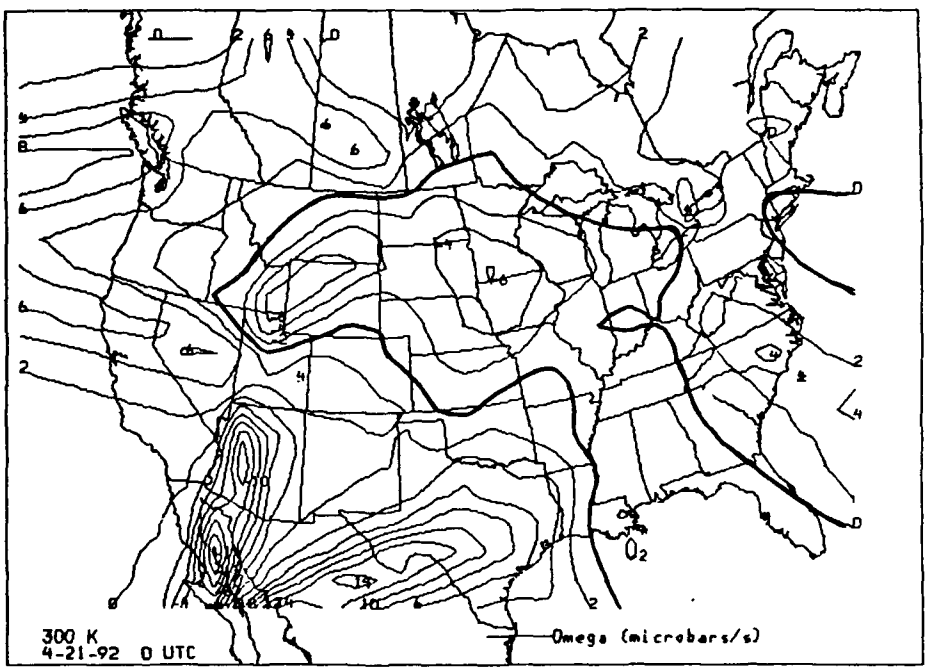

Fig. 46 Same as Fig. 10, except for 0000 UTC 21 April 1992.

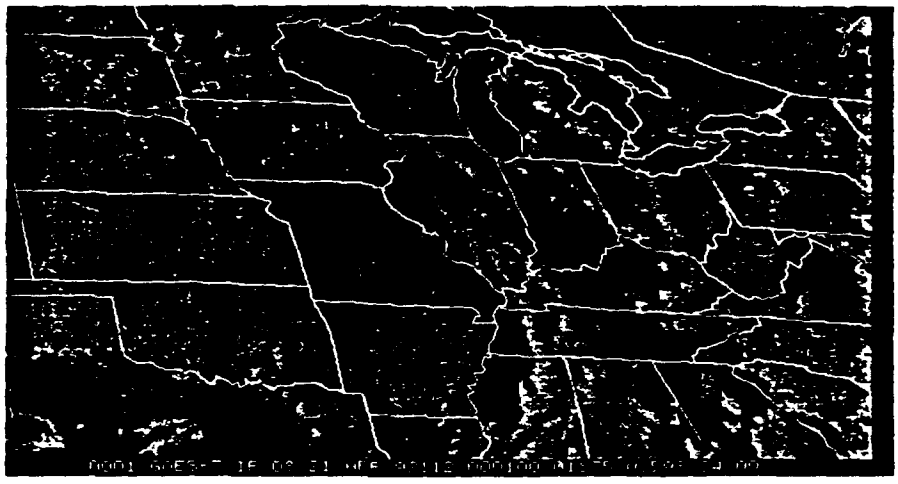

Fig. 47 Same as Fig. 20, except for 1800 UTC 20 April 1992.

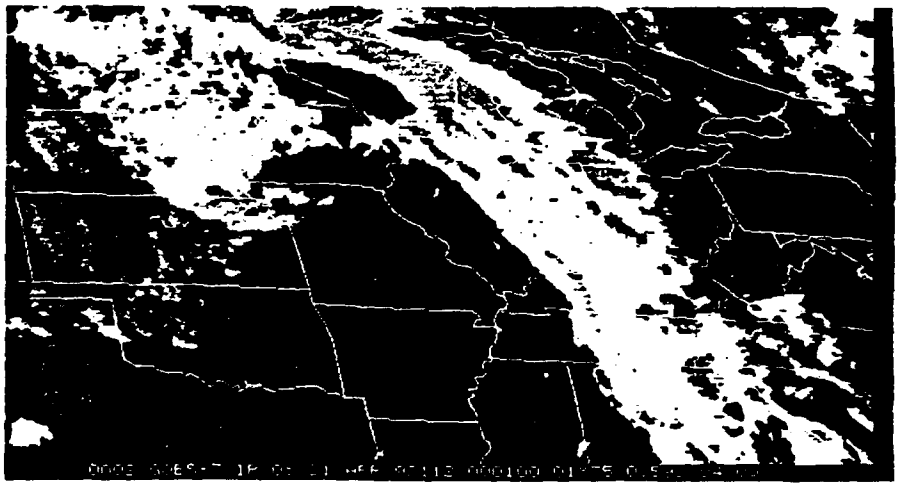

Fig. 48 Same as Fig. 21, except for 1800 UTC 20 April 1992.

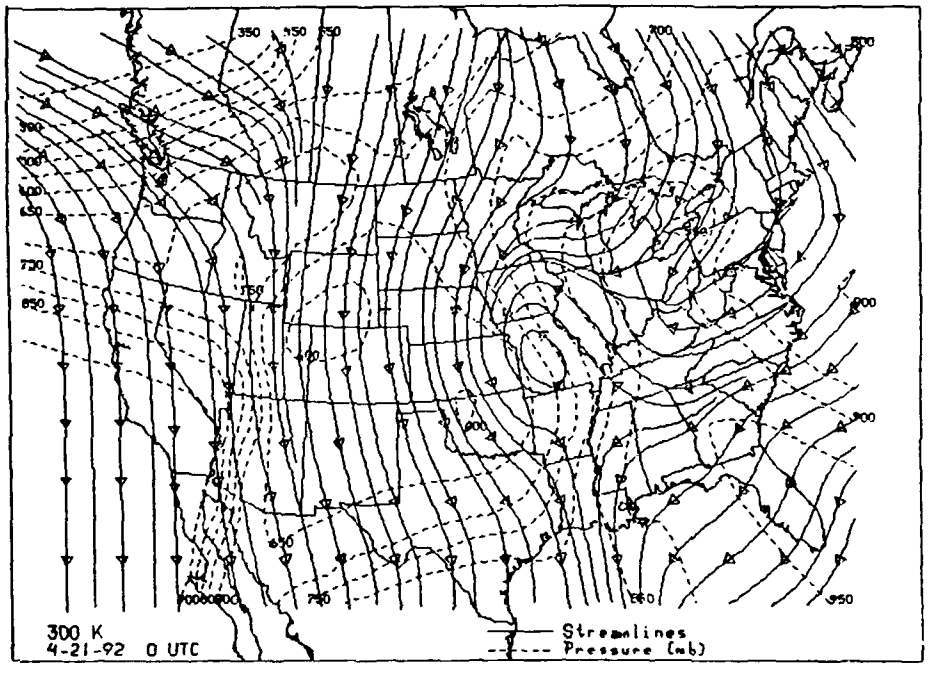

Fig. 49 Same as Fig. 12, except for 0000 UTC 21 April 1992.

4.4.3 Upper-Level Jet Secondary Ageostrophic Circulations

The 300 mb height and isotach chart for 0000 UTC 27 December (Fig. 50) shows a north - south jet streak over the upper Mississippi Valley with a jet core > 50 m s^{-1} (100 kts) over western Illinois. The jet exit region extends into northern Iowa.

The cross section of the tangential ageostrophic component of the wind and vertical motion (Fig. 51) for 0000 UTC 21 April along line I-J in Fig. 50 shows an indirect thermal circulation in the exit region of the jet streak. The values of UVM in Fig. 51 correlate well with the area of S-R vertical motion values, and both have approximately the same magnitude. This UVM also correlates well with the area of enhanced snowfall in the Omaha, Nebraska, area. Some of the heaviest snowfall rates were falling at 0000 UTC 21 April in the area of strongest UVM. Areas to the east were too warm in the boundary layer and received mostly rain.

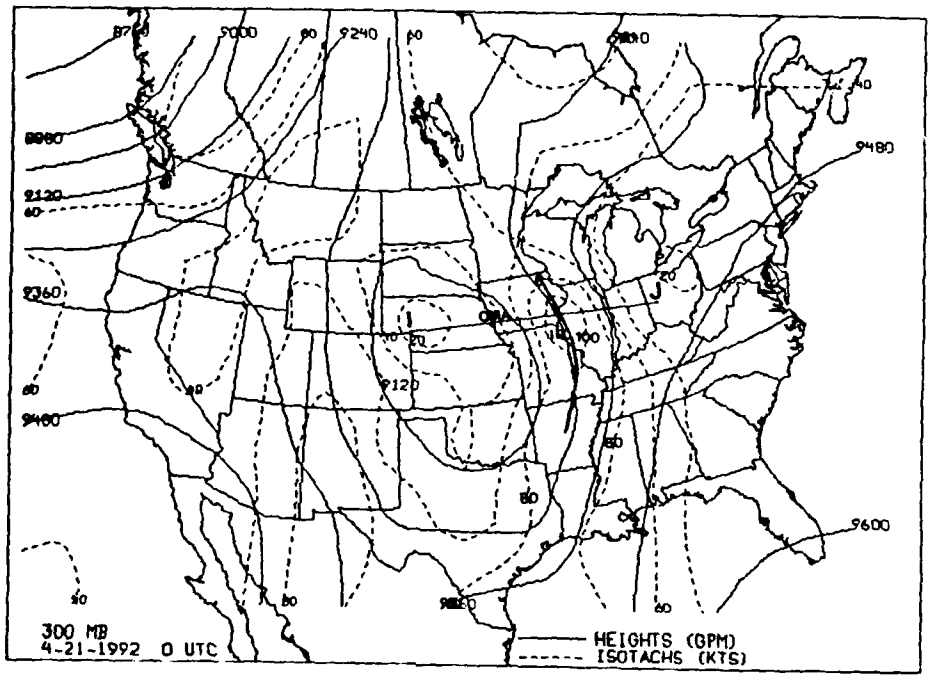

Fig. 50 Same as Fig. 22, except for 0000 UTC 21 April 1992. OMA = Omaha, Nebraska.

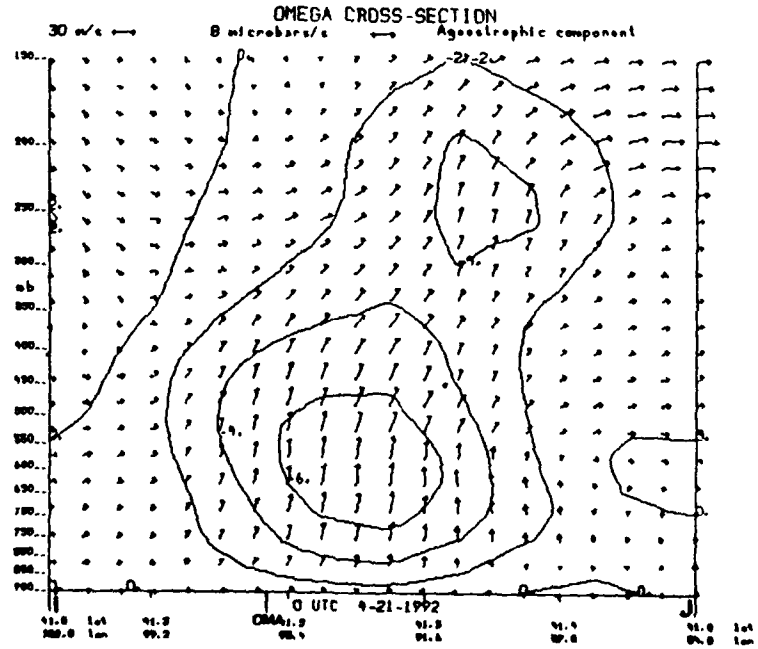

Fig. 51 Same as Fig. 28, except along line I-J in Fig. 50 for 0000 UTC 21 April 1992. OMA = Omaha, Nebraska.

4.5 Case 5: 13-16 December 1987

4.5.1 Synoptic Overview

A long wave trough developed in the upper air over the southwestern United States on 14 December 1987. On 15 December the trough lifted out and began to move rapidly into the central plains and mid-Mississippi River Valley (Fig. 52).

At the surface a weak low developed on 14 December over south-central Texas. By 0000 UTC 15 December the low had moved rapidly to the northeast and was centered over central Arkansas with a central pressure of 996 mb (Fig. 53). A cold front extended south from the low pressure center through Louisiana and eastern Texas. A warm front stretched northeast from the low's center through Tennessee and Kentucky. From 0000 UTC to 1200 UTC 15 December the storm moved from Arkansas to northeastern Illinois and the low deepened to 976 mb (Fig. 53).

The storm produced heavy snow from northern Texas to Michigan (Fig. 54). There were several reports of thunder and frozen precipitation associated with this storm.

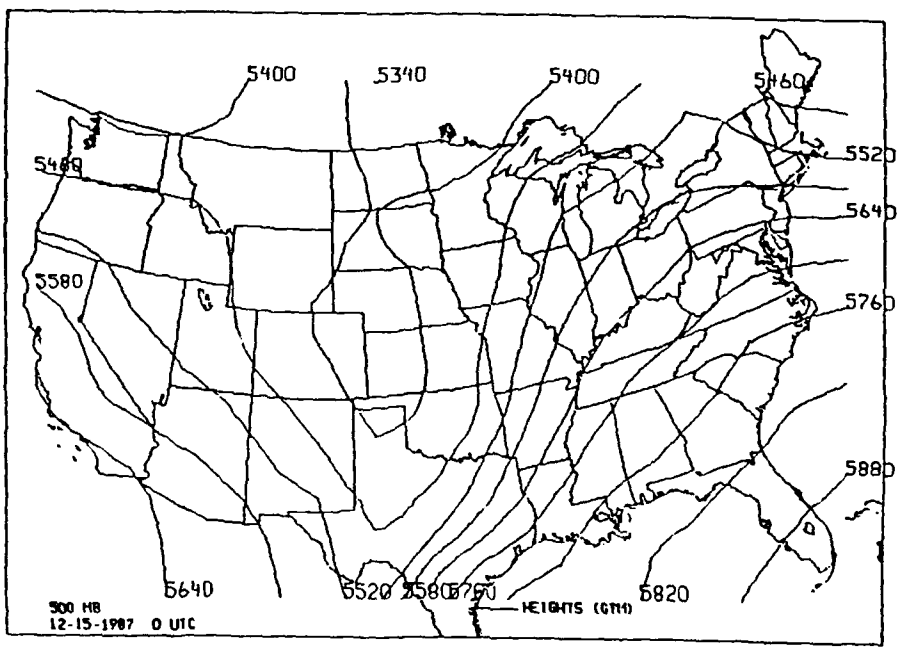

Fig. 52 500 mb chart for 0000 UTC 15 December 1987.

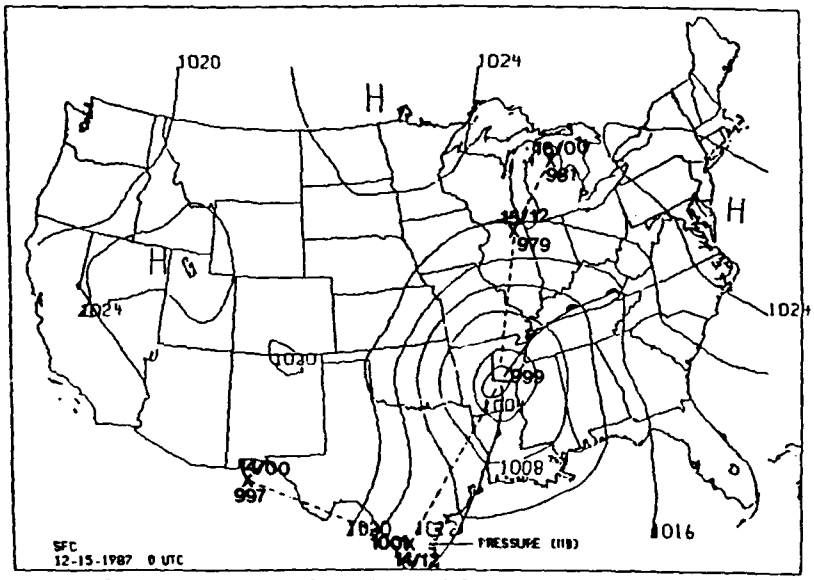

Fig. 53 Surface analysis for 0000 UTC 15 December 1987. Pressure in millibars. X's mark position of surface low and pressure in time from 0000 UTC 14 December to 0000 UTC 16 December 1987.

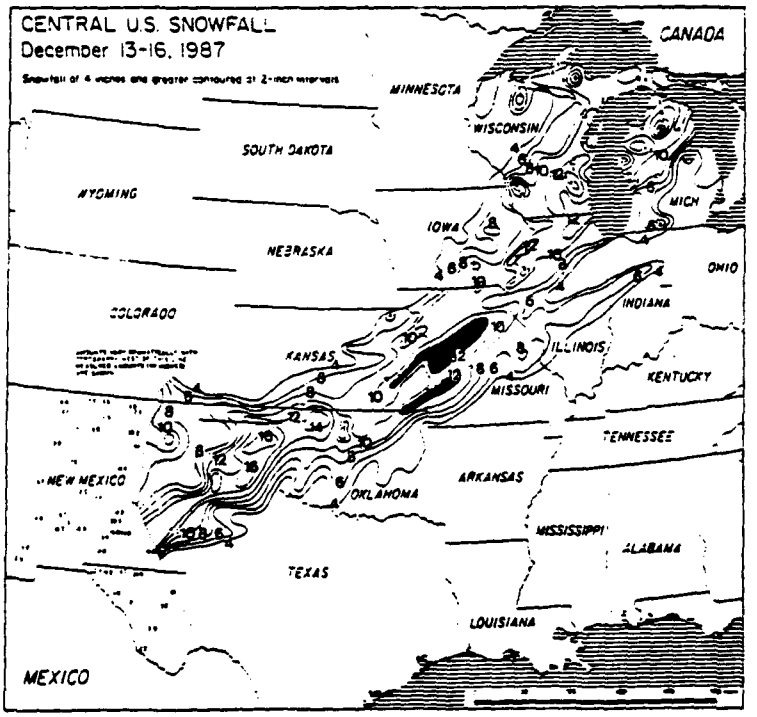

Fig. 54 Snowfall totals (inches) over the central United States from 13 to 16 December 1987. Blackened areas in west-central and southwest Missouri indicate 12 inch isopleths. (Storm Data December 1987).

4.5.2 Elevated Convection

As discussed earlier, the meteorologist must discriminate between regions of CSI and convective instability. CSI and convective instability may co-exist, but convective instability will dominate due to its faster growth rate. Fig. 55 shows the 850-300 mb thickness pattern for 0000 UTC 15 December and the location of the cross section labeled K-L, used for this case. This line was selected because several stations in the vicinity (Joplin (JLN) and Springfield (SGF), Missouri, and Harrison (HRO), Arkansas) reported thunder and frozen precipitation at or around 0000 UTC 15 December.

Term 1 of (9) (Fig. 56) reveals mostly negative values with a larger negative area extending into the upper levels. Term 2 of (9) (Fig. 57) along the same cross section displays mostly positive values with the exception of a large negative region sloping northward along the warm front. This negative region denotes convective instability, since term 2 will be < 0 only in convectively unstable areas. In this region upright convection is favored over slantwise convection due to a greater growth rate. Soundings from Monett (UMN), Missouri, and Topeka (TOP), Kansas, (not shown), reveal

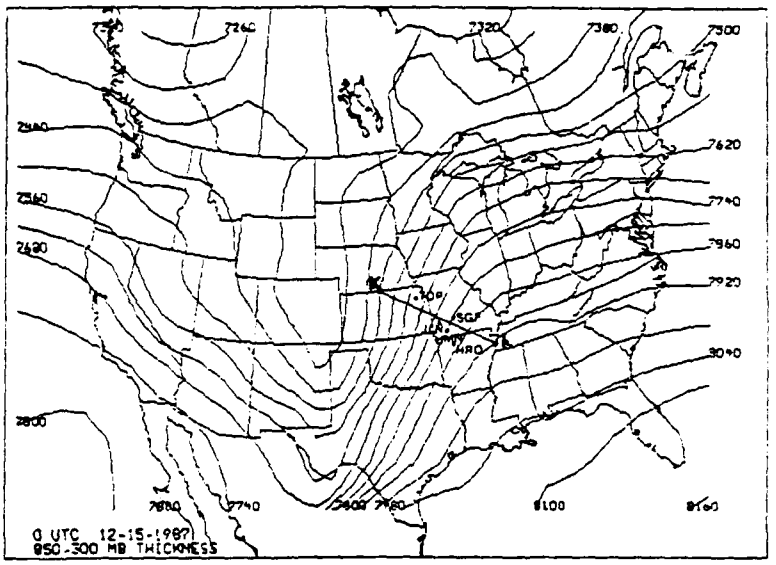

Fig. 55 Same as Fig. 13, except for 0000 UTC 15 December 1987. Three letter station identifiers at filled circles are Joplin (JLN), MO, Springfield (SGF), MO, Harrison, (HRO), AR, Topeka (TOP), KS, Monett (UMN), MO.

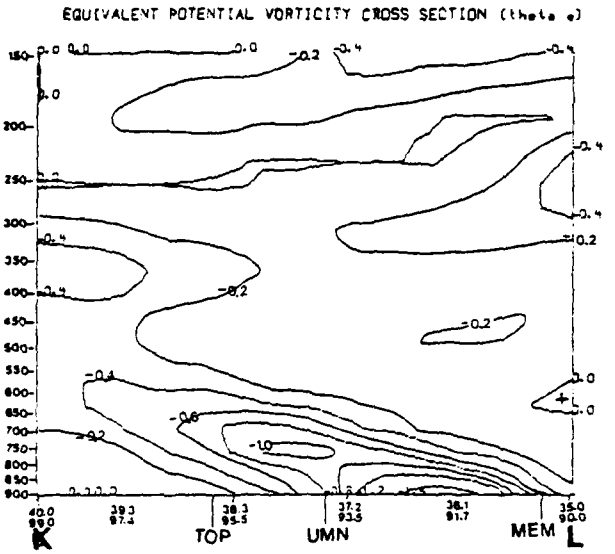

Fig. 56 Same as Fig. 14, except along line K-L in Fig. 55 for 0000 UTC 15 December 1987. TOP = Topeka, Kansas, UMN = Monett, Missouri, MEM = Memphis, Tennessee.

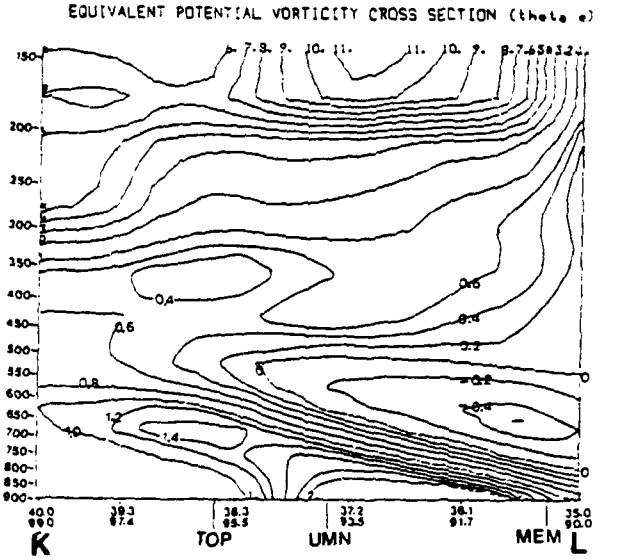

Fig. 57 Same as Fig. 15, except along line K-L in Fig. 55 for 0000 UTC 15 December 1987. TOP = Topeka, Kansas, UMN = Monett, Missouri, MEM = Memphis, Tennessee.

the mean relative humidity exceeded 85% from the surface to 540 mb at this time. The negative region with high moisture availability in the low and mid-levels north of the warm front indicates areas of elevated convection.

Fig. 58 shows the total EPV field for cross section K-L. The convectively unstable region is stippled to indicate the region favoring elevated upright convection and not CSI. However, as Moore and Lambert (1993) discussed, it is possible that the elevated upright convection was organized and modified by the slantwise convection, since the snowfall totals from this storm do reveal a banded structure. CSI exists only between 350-400 mb in an area to the north. This area is relatively shallow and quite high in the troposphere (where the relative humidity is lower and vertical motions are likely weaker), indicating CSI is unlikely to have contributed to the precipitation. In this case, EPV needs to be used with care since CSI can co-exist with convective instability, but convective instability typically dominates.

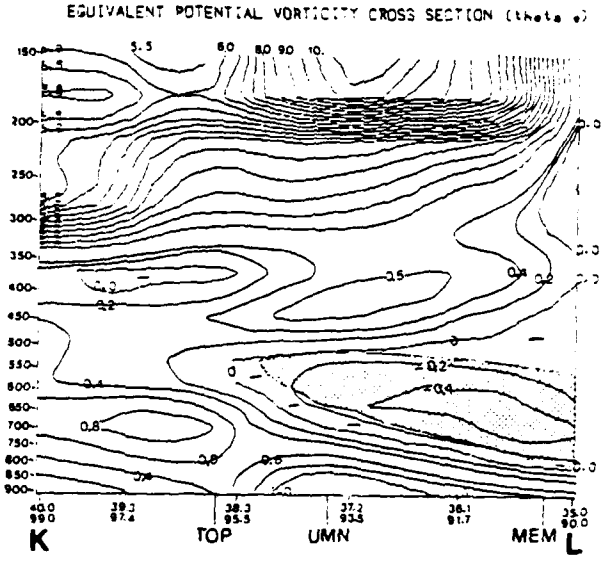

Fig. 58 Same as Fig. 16, except along line K-L in Fig. 55 for 0000 UTC 15 December 1987. TOP = Topeka, Kansas, UMN = Monett, Missouri, MEM = Memphis, Tennessee. Stippled region denotes convective instability.

5. CONCLUSIONS

The five case studies presented provide an opportunity to study the initiation and development of MPSs that organize within macro β scale ETCs. Several other cases were investigated to increase our understanding of the associated forcing mechanisms but were not included for detailed analysis in this thesis. The investigative findings support the major objective of this research, which is to analyze the role of select forcing mechanisms in the initiation and development of MPSs. Synoptic scale datasets were used to develop techniques to diagnose those forcing mechanisms which lead to MPS development.

Each of the cases contained one or more of the forcing mechanisms initially believed to be responsible for developing MPSs and their accompanying heavy snowfall. This research found that in areas of snowfall greater than 10 cm (4 in) one or more of the forcing mechanisms existed. The primary forcing mechanism(s) for each case is listed:

SNOW CASE	FORCING MECHANISMS
1) Colorado	S-R isentropic vertical motions CSI
2) Minnesota	S-R isentropic vertical motions Frontogenetical forcing

	Upper-level jet secondary ageostrophic circulations
3) Eastern Missouri	S-R isentropic vertical motions Upper-level jet secondary ageostrophic circulations CSI
4) Eastern Kansas - Nebraska	S-R isentropic vertical motions Upper-level jet secondary ageostrophic circulations
5) Central US	Elevated convection

Isentropic analysis was used in this research to gain a better insight into the three-dimensional motions of the atmosphere. S-R isentropic vertical motion and streamlines were generated and compared to the G-R isentropic motion fields. In each case S-R values were found to represent atmospheric vertical motions and flow patterns more accurately than G-R and standard pressure representations of the atmosphere. S-R omegas were stronger and more accurately placed with respect to cloud features. S-R streamlines revealed flow regimes of greater lifting within the storm and the direction of inflow into the storm. S-R isentropic vertical motions and streamlines provide a "3-D" view of the enhanced forcing within the large scale where the MPS formed.

EPV was computed within a cross sectional plane to diagnose the storms for CSI. Values of EPV < 0 in a convectively stable atmosphere indicate regions of CSI.

Given sufficient moisture and upward vertical motion, regions of CSI result in heavy precipitation bands that tend to be oriented parallel to the thickness field. This is confirmed by the use of Doppler radar reflectivities.

Since CSI and convective instability can co-exist, both terms comprising EPV were examined to diagnose convectively unstable regions. In the latter regions upright convection will dominate over slantwise convection, often creating elevated convection and heavy frozen precipitation events. It is also possible to have elevated convection in regions of weak conditional symmetric stability given sufficient frontogenetical forcing. EPV diagnosis is useful in identifying either case.

Frontogenesis was computed in mid-tropospheric levels to confirm the existence of a sloping zone of frontogenesis acting on a front. Cross sections of the tangential ageostrophic circulation in the area of heavy precipitation revealed that a DTC did form coincident with frontogenesis and that the strongest UVM was located south of the axis of maximum frontogenesis.

Cross sections of the tangential ageostrophic component of the wind and vertical motion were generated to detect thermal circulations associated with jet streaks, also. Transverse circulations associated with separate jet streaks were identified and observed to merge, thus focusing a region of ascent, contributing to the rapid development of heavy snow. Also, the transverse circulation associated with either the exit or entrance region of a jet was seen to enhance the area of UVM produced by other forcing mechanisms.

There are several limitations to the results of this thesis. The poor spatial and temporal resolution of the upper air data resulted in using synoptic scale data to identify the various forcing mechanisms, which are mesoscale processes. Another problem was the limited number of cases. Although the cases studied indicate a direct relationship between the existence of the forcing mechanisms in an area of enhanced frozen precipitation, the number of cases was far too small to allow sweeping generalizations about whether the relationships exist in all or even most cases.

The fact that each of the forcing mechanisms contributing to MPS events is resolvable in the existing synoptic network and that the developed

diagnostic techniques could identify the forcing mechanisms is very encouraging. Further research is needed to increase the size of the case study data base to establish whether the relationships between the various forcing mechanisms and MPS heavy precipitation events exist in a statistically significant number of cases. Also, using data with better spatial and temporal resolution from new sources becoming available, such as Doppler radar, wind profilers, and mesoscale numerical model data, will improve our ability to resolve these mesoscale phenomena.

It is hoped these diagnostic techniques will be applied in a prognostic setting. Operational meteorologists today could use numerical model data with data handling and display software like the Personal Computer Gridded Interactive Display and Diagnostic System (PC-GRIDDS) to generate forecast elements of these diagnostic techniques. In the future, these techniques could be used with operational mesoscale model data to improve our ability to forecast MPSs and the resulting heavy frozen precipitation.

BIBLIOGRAPHY

Barnes, S. L., 1973: Mesoscale Objective Map Analysis Using Weighted Time-Series Observations. NOAA Tech. Memo. ERL NSSL-62, 1-9.

Beckman, S. K., 1987: Use of Enhanced IR/Visible Satellite Imagery to Determine Heavy Snow Areas. Mon. Wea. Rev., 115, 2060-2087.

Bennetts, D. A., and B. J. Hoskins, 1979: Conditional Symmetric Instability - A Possible Explanation for Frontal Rainbands. Quart. J. Roy. Meteor. Soc., 105, 945-962.

____, and J. C. Sharp, 1982: The Relevance of Conditional Symmetric Instability to the Prediction of Mesoscale Frontal Rainbands. Quart. J. Roy. Meteor. Soc., 108, 595-602.

Bluestein, H., 1986: Fronts and Jet Streaks: A Theoretical Perspective. Chap. 9 - Mesoscale Meteorology and Forecasting, ed. by Peter Ray, Amer. Meteor. Soc., Boston, MA, 173-215.

Boyle, J. S., and L. F. Bosart, 1986: Cyclone-Anticyclone Couplets over North America. Part II: Analysis of a Major Cyclone Event over the Eastern United States. Mon. Wea. Rev., 114, 2432-2465.

Browning, K. A., 1986: Conceptual Models of Precipitation Systems. Wea. Forecasting, 1, 23-40.

Byrd, G. P., 1989: A Composite Analysis of Winter Season Overrunning Precipitation Bands over the Southern Plains of the United States. J. Atmos. Sci., 46, 1119-1132.

Carlson, T. N., 1980: Airflow Through Midlatitude Cyclones and the Comma Cloud Pattern. Mon. Wea. Rev., 108, 1498-1509.

____, 1991: Mid-Latitude Weather Systems. Harper-Collins Academic, New York, 507 pp.

Colman, B. R., 1990: Thunderstorms Above Frontal Surfaces in Environments Without Positive CAPE. Part I: A Climatology. Mon. Wea. Rev., 118, 1103-1121.

_____, 1990: Thunderstorms Above Frontal Surfaces in Environments Without Positive CAPE. Part II: Organization and Instability Mechanisms. Mon. Wea. Rev., 118, 1123-1144.

Daily Weather Maps, National Oceanic and Atmospheric Administration (NOAA), Climatic Analysis Center, December 1990.

Daily Weather Maps, National Oceanic and Atmospheric Admisnistration (NOAA), Climatic Analysis Center, April 1992.

Dunn, L. B., 1992: Evidence of Ascent in a Sloped Barrier Jet and an Associated Heavy-Snow Band. Mon. Wea. Rev., 120, 914-924.

Duquet, R. L., 1964: Data Processing for Isentropic Analysis, USAEC Report TID-21609. Pennsylvania State University, PA, 36 pp.

Elkins, H. A., 1987: Thunderstorms with Snow: A Comprehensive, Empirical Study of Their Occurrence, Development and Structure. MS Thesis, Saint Louis University, MO, 79 pp.

Emanuel, K. A., 1983: The Lagrangian Parcel Dynamics of Moist Symmetric Instability. J. Atmos. Sci., 40, 2368-2376.

_____, 1985: Frontal Circulation in the Presence of Small Moist Symmetric Stability. J. Atmos. Sci., 42, 1062-1071.

Funk, T. W., 1991: Forecasting Techniques Utilized by the Forecast Branch of the National Meteorological Center During a Major Convective Rainfall Event. Wea. Forecasting, 6, 548-564.

Gyakum, J. R., 1987: Evolution of a Surprise Snowfall in the United States Midwest. Mon. Wea. Rev., 115, 2322-2345.

Hakim, G. J., and L. W. Uccellini, 1992: Diagnosing Coupled Jet-Streak Circulations for a Northern Plains Snow Band from Operational Nested-Grid Model. Wea. Forecasting, 7, 26-47.

Haltiner, G. J., and F. L. Martin, 1957: Dynamical and Physical Meteorology. McGraw-Hill, New York, NY, 470 pp.

Harrold, T. W., 1973: Mechanisms Influencing the Distribution of Precipitation within Baroclinic Disturbances. Quart. J. Roy. Meteor. Soc., 99, 232-251.

Hobbs, P. V., 1978: Organization and Structure of Clouds and Precipitation on the Mesoscale and Microscale in Cyclonic Storms. Rev. Geophys. Space Phys., 16, 741-755.

Holton, J. R., 1979: An Introduction to Dynamic Meteorology. Academic Press, NY, 391 pp.

Hoskins, B. J., I. Draghici, and H. C. Davies, 1978: A New Look at the Omega Equation. Quart. J. Roy. Meteor. Soc., 104, 31-38.

____, and M. A. Pedder, 1980: The Diagnosis of Middle Latitude Synoptic Development. Quart. J. Roy. Meteor. Soc., 106, 707-719.

Houze, R. A., P. V. Hobbs, K. R. Biswas and W. A. Davis, 1976: Mesoscale Rainbands in Extratropical Cyclones. Mon. Wea. Rev., 104, 868-878.

Kocin, P. J., L. W. Uccellini, J. W. Zack, and M. L. Kaplan, 1985: A Mesoscale Numerical Forecast of an Intense Convective Snowburst Along the East Coast. Bull. Amer. Meteor. Soc., 66, 1412-1424.

Lilly, D. K., 1986: Instabilities. Chap. 11 - Mesoscale Meteorology and Forecasting, ed. by Peter Ray, Amer. Meteor. Soc., Boston, MA, 261-264.

Martin, J. E., J. D. Locatelli, and P. V. Hobbs, 1992: Organization and Structure of Clouds and Precipitation on the Mid-Atlantic Coast of the United States. Part V: The Role of an Upper-Level Front in the Generation of a Rainband. J. Atmos Sci., 49, 1293-1303.

Matejka, T. J., R. A. Houze, and P. V. Hobbs, 1980: Microphysics and Dynamics of Clouds Associated with Mesoscale Rainbands in Extratropical Cyclones. Quart J. Roy. Meteor. Soc., 106, 29-56.

Miller, J. E., 1948: On the Concept of Frontogenesis. J. Meteor., 11, 169-171.

Molinaro, R. C., 1988: Diagnostic and Kinematic Fields Associated with Curved and Straight Jet Streaks Using a Two-Layer Primitive Equation Model. Ph.D. dissertation, Saint Louis University, MO, 207 pp.

Moore, J. T., and P. D. Blakely, 1988: The Role of Frontogenetical Forcing and Conditional Symmetric Instability in the Midwest Snowstorm of 30-31 January 1982. Mon. Wea. Rev., 116, 2155-2171.

____, 1992: Isentropic Analysis and Interpretation: Operational Applications to Synoptic and Mesoscale Forecast Problems. Air Weather Service, AWS/TN-87/002, revised 1989, 87 pp.

____, and T. E. Lambert, 1993: The Use of Equivalent Potential Vorticity to Diagnose Regions of Conditional Symmetric Instability. Wea. Forecasting. Accepted for publication.

____, and G. E. VanKnowe, 1992: The Effect of Jet-Streak Curvature on Kinematic Fields. Mon. Wea. Rev., 120, 2429-2441.

O'Brien, J. J., 1970: Alternative Solutions to the Classical Vertical Velocity Problem. J. Appl. Meteor., 9, 197-203.

Palmen, E., and C. W. Newton, 1969: Atmospheric Circulation Systems. Academic Press, NY, 603 pp.

Petterssen, S., 1936: Contribution to the Theory of Frontogenesis. Geof. Pub., 11, No. 6, 1-27.

Rasmussen, R., M. Politovich, J. Marwitz, W. Sand, J. McGinley, J. Smart, R. Pielke, S. Rutledge, D. Wesley, G. Stossmeister, B. Bernstein, K. Elmore, N. Powell, E. Westwater, B. B. Stankov, and D. Burrows, 1992: Winter Icing and Storms (WISP). Bull. Amer. Meteor. Soc., 73, 951-974.

Sanders, F., and L. F. Bosart, 1985: Mesoscale Structure in the Megalopolitan Snowstorm of 11-12 February 1983. Part I: Frontogenetical Forcing and Symmetric Instability. J. Atmos. Sci., 42, 1050-1061.

Saucier, W., 1955: Principles of Meteorological Analysis. University of Chicago Press, Chicago, IL, 438 pp.

Scofield, R. A., and J. Robinson, 1990: Using Instability Bursts and Satellite Imagery to Analyze and NOWCAST Heavy Snow. Satellite Application Information Note 90/1, NESDIS, Washington, DC.

Shapiro, M. A., and P. J. Kennedy, 1981: Research Aircraft Measurements of Jet Stream Geostrophic and Ageostrophic Winds. J. Atmos. Sci., 38, 2642-2652.

Shields, M. T., R. M. Rauber, and M. K. Ramamurthy, 1991: Dynamical Forcing and Mesoscale Organization of Precipitation Bands in a Midwest Winter Cyclonic Storm. Mon. Wea. Rev., 119, 936-964.

Snook, J. S., 1992: Current Techniques for Real-Time Evaluation of Conditional Symmetric Instability. Wea. Forecasting, 7, 430-439.

Storm Data, 1987: National Climatic Data Center, NOAA, 29, (December), Asheville, NC, 44 pp.

Storm Data, 1991a: National Climatic Data Center, NOAA, 33, (January), Asheville, NC, 60 pp.

Storm Data, 1991b: National Climatic Data Center, NOAA, 33, (October), Asheville, NC, 74 pp.

Storm Data, 1991c: National Climatic Data Center, NOAA, 33, (November), Asheville, NC, 57 pp.

Uccellini, L. W., 1976: Operational Diagnostic Applications of Isentropic Analysis. Nat. Wea. Dig., 1, 4-12.

____, and P. J. Kocin, 1987: The Interaction of Jet Streak Circulations During Heavy Snow Events Along the East Coast of the United States. Wea. Forecasting, 2, 289-308.

Wang, P. Y., D. B. Parsons, and P. V. Hobbs: The Mesoscale and Microscale Structure and Organization of Clouds and Precipitation in Midlatitude Cyclones. VI: Wavelike Rainbands Associated With a Cold-Frontal Zone. J. Atmos. Sci., 40, 543-558.

Wolfsberg, D. G., K. E. Emanuel, and R. E. Passarelli, 1986: Band Formation in a New England Winter Storm. Mon. Wea. Rev., 114, 1552-1569.

BIOGRAPHY OF THE AUTHOR

Mark Arthur Kaster was born on May 15, 1958, in Sibley, Iowa, to Mr. and Mrs. Arthur L. Kaster. He grew up on a farm in Northwest Iowa and graduated from George Community High School, George, Iowa, in 1976. After graduation he joined the Iowa Army National Guard and served in the infantry for four years. In December 1982 he received a Bachelor of Science degree in Meteorology from Iowa State University.

In 1984 he received his commission from the United States Air Force Officer Training School. From 1984 through 1986 he served as the Wing Weather Officer to the 319th Strategic Bombing Wing and the 321st Strategic Missile Wing at Grand Forks AFB, North Dakota. From 1986 through 1989 he was the Officer in Charge of the US Army's 3rd Armored Division Tactical Weather Team at Hanau Army Airfield, Germany. In 1989 he graduated from Troy State University with a Master of Science degree in Management. From 1989 through 1992 he served as a staff officer at Headquarters Air Weather Service, Scott AFB, Illinois. In 1992 he was assigned to complete a Master of Science degree in Meteorology at Saint Louis University. He is married to the former Tracy Ann Kirk. They have two daughters, Amanda and Abigail.